THE ASTROPHYSICAL JOURNAL, 197: 551–570, 1975 May 1

THE EVOLUTION OF GALAXIES. IV. HIGHLY FLATTENED DISKS

RAYMOND J. TALBOT, JR.
Department of Space Physics and Astronomy, Rice University
AND
W. DAVID ARNETT
University of Texas at Austin
Received 1974 July 1; revised 1974 November 13

ABSTRACT

We present computations of the structure and evolution of models of the disk component of galaxies. The models display the qualitative characteristics and the statistically dominant trends observed in late-type spirals. The radial distributions of neutral hydrogen, of H II regions, and of colors are well reproduced. We find composition gradients across the faces of disk models. Using the observed supernova rates in spirals, these models place fairly severe constraints upon the progenitors of supernova. If azimuthally averaged, high-resolution observations of neutral hydrogen will provide interesting quantitative tests of models of this type.

Equations governing the structure and evolution of our models of the disk components are discussed in detail, as are the uncertainties in input physics and astronomy.

Subject headings: galactic structure — stellar dynamics — stellar evolution

I. INTRODUCTION

A theoretical description of the evolution of a galaxy requires the specification of initial conditions for the various constituents, prescriptions for star formation and the ejecta from stars, and a scheme for following the properties of the system in time and space. Early investigations of this problem (Salpeter 1955, 1959; Schmidt 1959, 1963; Limber 1960; Tinsley 1968, 1972; Truran and Cameron 1971; Talbot and Arnett 1971, 1973*a*, *b*) considered the case of an initial mixture of gas (or gas plus stars) contained in a single *fixed volume* with constant total mass density. This simplification, which we shall call the one-zone model, allows formulation of the problem with time as a single independent variable.

Various degrees of agreement have been found between those models and observations of the integral properties of galaxies; however, no detailed theoretical investigation of the observed spatial variations in galaxies is possible within this context. Schmidt (1959) discussed the approximate behavior of the gas density and other properties as a function of distance from the Galactic center. In particular, he used the observed fact that gas-density variations with radius are small (in contrast to the large variation of the total density) to argue against the stellar birthrate being proportional to only the first power of the gas density. Current observational efforts on several fronts are making available many detailed data on spatial variations in galaxies, which should provide the basis for much more significant constraints on models.

This paper presents the temporal and spatial structure and evolution of highly flattened model galaxies. We are not here attempting to construct models of specific classes of galaxies. Many of the approximations and uncertainties of the one-zone models are still with us. Specifically, the stellar birth and death processes are not well understood, and the initial conditions for galaxies are not known. We assume that cylindrical shells of a galaxy each evolve independently of the rest; this allows an evolutionary model to be built from a superposition of a set of one-zone calculations. For this paper we have adopted a simplified model of the mass distribution in flattened galaxies. The prescriptions applied to these simple models may easily be generalized to specific mass distributions for specific galaxies. Our simplifying assumptions in this paper preclude an accurate consideration of processes which occur during an initial collapse phase such as discussed by Eggen, Lynden-Bell, and Sandage (1962) and by Larson (1974).

For our models of disk galaxies we present the radial variation of dependent variables. One and only one independent variable is changed with radius—the total mass per unit area at r, $\sigma(r)$. With respect to the radial coordinate we do not vary assumptions about stellar evolution or the initial mass function of star formation (IMF), nor do we posit any arbitrary mass flow in or out of portions of the system. No parameters are adjusted to achieve the radial variation in mass-to-light ratios, colors, compositions, supernova rates, or surface mass density of gas. To produce a sequence of models which display many of the qualitative features of flat disk galaxies, we vary only the central surface mass density of the disk.

We do not emphasize the discussion in the previous paragraph because the simple models presented here are satisfactory representations of real disk galaxies in all respects; they are incomplete. We emphasize the variation of the single parameter with radius because the prior discussion of the radial variation of the mass-to-light ratio by Quirk and Tinsley (1973) and Tinsley (1973) employed ad hoc assumptions about the varia-

tion of the lower mass limit to the IMF. This parameter was varied as required to fit the observations. Our point is that we are varying only one quantity, and it is a quantity which is independently known and one whose value is probably controlled by initial conditions at the time the galaxy formed. The variation must be included in any model before one can say for certain that a constant initial mass function is inadequate. Furthermore, the physics of the support of the disk against its gravitational field governs the properties of the gas which in turn governs the rate of star formation and perhaps the form of the initial mass function. It is necessary to have models of such disks before one can ascertain the proper *physical* prescription for a variable initial mass function if it should be evident that a constant IMF is inadequate.

In order to fit any specific disk galaxy one may employ our basic model and fit the observations of that galaxy by (1) employing a mass distribution which gives the observed rotation curve and (2) prescribing the physics of star formation to achieve the proper mass-to-light ratio, colors, and compositions at each radius. The latter may include varying the IMF and/or mass flow.

Section II discusses the construction of our simplified model of a highly flattened galaxy. Section III contains the prescription for applying the one-zone results to this model. Section IV gives some results obtained with several prescriptions for the rate of star formation. Section V presents detailed results for one of the prescriptions. The radial variations of quantities are displayed and the integrated properties of the models are discussed; there is a brief discussion of the comparison between observations and the models. Section VI discusses the relationship between our model disk galaxies and real galaxies, pointing out the directions for future improvements in the models and those aspects of our results which are insensitive to the details of the current model.

II. THE STANDARD FLATTENED EXPONENTIAL GALAXY (SFEG) MODEL

Our purpose in this paper is to discuss the evolutionary behavior of general, highly-flattened model galaxies. Consequently it will be expedient to employ a simple, but fairly realistic, model for the distribution of surface mass density σ over the face of the disk of flattened galaxies. We adopt the exponential form

$$\sigma(r) = \sigma_0 \exp(-r/R), \tag{1}$$

where r is the radial distance from the axis of rotation and σ_0 and R are the two parameters which give a two-parameter family of models. This choice was based upon the observed exponential variation of the surface brightness of disk galaxies (e.g., de Vaucouleurs 1959; Freeman 1970) and the arguments by Nordsieck (1973*a*, *b*) that the mass-to-light ratio is constant in disks. The observational argument for an exponential *mass* distribution is not strong, and there is no justification for using it to extrapolate to large r. For our goal of making model galaxies we find equation (1) to be a satisfactory and convenient method of presenting general results while simultaneously having an approximately correct form. If we were to construct models of specific galaxies, $\sigma(r)$ would be determined by fitting observed rotation curves.

Although for many real spiral galaxies the flattened-disk approximation breaks down in the central bulge region, for our purposes in this paper the central bulge may be represented by a surface mass density higher than that given by equation (1): i.e., a bulge (B) corresponds to $\sigma(0) = \sigma_B > \sigma_0$.

For the disk described by equation (1), the total mass is $\mathcal{M}_D = 2\pi R^2 \sigma_0$ where we append the subscript D to distinguish this from the total mass of galaxy which, in general, would include the bulge mass $\mathcal{M}_B$.

For a system with a single fluid, the well-known plane-parallel solution for the volume density ρ is (Spitzer 1942; Ledoux 1951; Vandervoort 1970*a*)

$$\rho(z) = \rho' \operatorname{sech}^2(z/W), \tag{2}$$

where ρ' is the total mass density at $z = 0$ and

$$W = v(2\pi G\rho')^{-1/2}; \tag{3}$$

v is the *effective* one-dimensional velocity dispersion (assumed independent of z) such that the fluid pressure $p = \rho v^2$, and the effective thickness is

$$2W = \sigma/\rho'. \tag{4}$$

The term "effective velocity" is used to allow for the gas to be supported in part by magnetic-field and cosmic-ray pressure, giving an effective gas pressure greater than the pressure arising from actual mass motion (cf. Kellman 1972).

If there is more than one fluid species (e.g., different types of stars or interstellar gas) each with its own velocity dispersion v_i^2, then the plane-parallel system satisfies

$$\frac{1}{\rho_i}\frac{dp_i}{dz} = v_i^2 \frac{d\ln\rho_i}{dz} = \frac{d\phi}{dz} \tag{5}$$

so that

$$\rho_i(z) = \rho_i(0) \exp\{v_i^{-2}[\phi(z) - \phi(0)]\}, \tag{6}$$

and the gravitational potential ϕ is computed from

$$\frac{d^2\phi}{dz^2} = -4\pi G \sum_i \rho_i(z). \tag{7}$$

By expansion about $z = 0$ (and employing the symmetry about $z = 0$) one obtains

$$\phi(z) - \phi(0) = -(2\pi G\rho')z^2\left\{1 - z^2\left[\frac{\pi G}{3}\sum_i \frac{\rho_i(0)}{v_i^2}\right] + \cdots\right\}, \tag{8}$$

where

$$\rho' = \sum_i \rho_i(0). \tag{9}$$

Therefore, the profile of the density near $z = 0$ is represented by

$$\rho_i(z) \simeq \rho_i(0) \exp\left[-(z/W_i)^2\right], \quad (10)$$

where

$$W_i = v_i(2\pi G\rho')^{-1/2}, \quad (11)$$

in analogy with equation (3).

It is clear that an expression for $\rho_i(z)$ can be obtained which is more precise than equation (10); however, for our purposes this approximation will be quite adequate. If equation (10) were precise, the effective thickness for species i would be

$$\sigma_i/\rho_i(0) = \pi^{1/2} W_i \quad (12)$$

which is $(\pi/4)^{1/2} = 0.886$ times the effective thickness if there were only a single species (eq. [4]). The higher-order terms in equation (8) will increase the effective thickness slightly, which tends to compensate for this. To a good approximation (a few percent error) we may always use $2W_i$ for the effective thickness.

We will need to evaluate the average value of ρ_i^κ integrated over z. For this the approximation of equation (10) is eminently well suited, giving

$$\int_0^\infty \rho_i^\kappa(z)dz \approx [\rho_i(0)]^\kappa(\pi/\kappa)^{1/2} W_i \quad (13)$$

or

$$\langle\rho_i^\kappa\rangle \approx \kappa^{-1/2}[\rho_i(0)]^\kappa . \quad (14)$$

All of these expressions have been developed for the plane-parallel case where physical quantities are independent of r. Vandervoort (1970*a*, *b*) has developed an extension of this kind of analysis by expansions in the ratio W/R where R is the characteristic scale-length in the r coordinate. Our expressions contain only terms corresponding to his zeroth-order terms for the density ρ and first-order term for the potential ϕ. Consequently, our approximations are restricted to "highly flattened galaxies," which means that the models contain only the leading terms in an expansion in W/R. Typically this ratio is about 0.1; hence, typical quantitative errors introduced by our use of plane-parallel relationships will be of order 10 percent or less. This will in no way affect the qualitative features which are the prime purpose of the simplified models developed here.

Finally, we collect some expressions useful when the set σ_i and v_i are given; we use $2W_i$ for the effective thickness always:

$$\nu'(r) \equiv [2\pi G\rho'(r)]^{1/2} = \pi G \sum_i \sigma_j(r)[v_j(r)]^{-1}, \quad (15)$$

$$W_i(r) = v_i(r)/\nu'(r), \quad (16)$$

$$\rho_i(r, 0) = \sigma_i(r)[2W_i(r)]^{-1}, \quad (17)$$

$$\langle\rho_i^\kappa\rangle \approx \kappa^{-1/2}[\rho_i(r, 0)]^\kappa, \quad (18)$$

$$\rho_i(r, z) \approx \rho_i(r, 0) \exp\{-[z/W_i(r)]^2\}, \quad (19)$$

$$p_i(r, z) = \rho_i(r, z)v_i^2(r). \quad (20)$$

The frequency ν' is related to the frequency of the oscillations of stars in the z-direction, ω_z, by $\omega_z = 2^{1/2}\nu'$.

III. METHOD OF CALCULATING EVOLUTIONARY BEHAVIOR

Our fundamental assumptions about galactic structure are that the surface mass density σ is a function only of the distance from the axis of symmetry r and that there is no mass flow in the r-direction. A direct consequence of this assumption is that material in an annular cylinder of radius r may be considered to evolve as an independent system, and therefore we may employ the results of one-zone computations, e.g., Talbot and Arnett (1971, 1973*a*, *b*; hereafter called TA71, TA73*a*, and TA73*b*).

Briefly, TA71 discussed the evolution of a unit mass of material $\mathcal{M}$ from interstellar gas into stars and subsequent ejection of a portion of that material back into the interstellar gas. The basic dependent variables are the set $\{\mathcal{M}_i, i = 1, i_{\max}\}$, where $\mathcal{M}_i$ is the portion of this unit mass in the form of interstellar gas of nuclear species i. The mass of the gas is $\mathcal{M}_g = \sum_i \mathcal{M}_i$, where the sum is from $i = 1$ to $i_{\max}$.

The total rate of conversion of gaseous mass into stars is given by a rate ν which is defined by

$$\left.\frac{d\mathcal{M}_g}{dt}\right|_* = -\nu\mathcal{M}_g \equiv \mathcal{B}(t); \quad (21)$$

the mass in a generation of stars is distributed among stars of mass m (in solar units) by prescribing an initial mass function (IMF) ψ_m. The form which we adopt is described in the Appendix.

The return of material (unprocessed and processed) to the interstellar medium is controlled by the lifetime τ_m of stars of mass m and the fraction of the mass of the star which is returned to the gas in the form of species i, R_{mi}. The values employed for τ_m and R_{mi} are the standard stellar evolution case discussed in TA73*a* and updated in Talbot and Arnett (1974; hereafter TA74). In the present version of the computer code R_{mi} is allowed to be a function of the composition from which the star formed, however τ_m is independent of the initial composition. Uncertainties in R_{mi} (see TA74) produce uncertainties in the production of heavy elements. This may produce a systematic shift of abundances up or down, but it will not alter the form of the computed distributions. See the Appendix also.

In general one may compute the dispersion velocity of the interstellar gas by solving an equation of the form

$$\frac{d}{dt}(\rho_g v_{g,\mathrm{turb}}^2) = (\text{turbulent velocity input by supernovae, OB stars, ...}) - (\text{turbulent velocity dissipation by cloud-cloud collisions....}) \quad (22)$$

and similar equations for the thermal velocity, magnetic field pressure, etc. The theory of the energy balance of the interstellar gas is currently uncertain,

and consequently it is not yet clear how to ascribe definite terms to the right-hand side of equation (22).

The qualitative nature of the energy generation and dissipation may be described by a schematic version of equation (22) for the effective gas dispersion $v_g^2 = v_{g,\mathrm{turb}}^2 + v_{g,\mathrm{ther}}^2 + \ldots$:

$$\frac{dv_g^2}{dt} = \nu V^2 - v_g^3/W_g = \nu V^2 - \nu' v_g^2 \qquad (23)$$

where $\frac{3}{2}V^2$ is the characteristic energy per unit mass imparted to the gas by young stars. We have assumed that the rate of generation of turbulence is proportional to the rate of star formation, and the dissipation process may be described by cloud-cloud collisions acting with a mean free path of W_g.

Equation (23) achieves equilibrium in a time of $1/\nu'$ which is the time for passage through the plane or the free-fall time. The equilibrium effective velocity is

$$(v_g^2)_{\mathrm{eq}} = V^2(\nu/\nu') . \qquad (24)$$

In a more thorough treatment one must consider the following problem: If the turbulent gas motions $v_{g,\mathrm{turb}}$ become supersonic, i.e., $v_{g,\mathrm{turb}} > v_{g,\mathrm{ther}}$, there will be enhanced dissipation. Also the equation for the thermal energy in the gas contains radiative terms which are very efficient for $T \gtrsim 10^4$ K. The upshot is that an attempt to raise $v_{g,\mathrm{turb}}$ above about $v_{g,\mathrm{ther}} = 9.1(T/10^4)^{1/2}$ km s^{-1} will be met by enhanced dissipation and T will not rise much above 10^4 K. The *effective* turbulent velocity v_g may obtain a value as high as about $\chi^{1/2} v_{g,\mathrm{ther}}$, where χ is the number of modes for energy equipartitioning; e.g., turbulent, thermal, magnetic field, and cosmic rays together may yield $\chi \approx 4$ and so a maximum effective velocity of

$$(v_g)_{\max} \equiv c \simeq 2 \times 9.1 = 18.2 \text{ km s}^{-1} .$$

By supersonic we will always mean gas velocities large relative to the H II thermal speed c.

As a rough qualitative statement we write

$$v_g^2 = \min (V^2\nu/\nu', c^2) . \qquad (25)$$

a) A Power-Law Model for the Birthrate of Stars

In order to develop simple analytic expressions and discuss a widely used parametrization, we follow Schmidt (1959) and investigate the following prescription for the rate of formation of stars:

$$\left.\frac{d\rho_g}{dt}\right|_* = -C\rho_g^{\kappa} , \qquad (26)$$

where C and κ are constants. We emphasize that this parametrization *assumes* that C and κ are *truly basic physical constants*, independent of time, position, or other physical quantities.

The surface density σ is a given function of r, and we assume that the z-distribution of the gas may be represented by equation (19). Integration of equation (26) over z yields

$$\left.\frac{d\sigma_g}{dt}\right|_* = -\nu\sigma_g , \qquad (27)$$

where

$$\nu(r) \approx C\kappa^{-1/2}[\rho_g(r, 0)]^{\kappa-1} ; \qquad (28)$$

$\nu(r)$ is in general a function of time also. In general the relationship between $\rho_g(r, 0)$ and σ_g involves the velocity v_g which in turn depends upon ν (eqs. [16], [17], [25], and [28]). We find

$$\nu = \{C\kappa^{-1/2}[\sigma_g(\nu')^{3/2}/2V]^{\kappa-1}\}^{2/(\kappa+1)} \quad \text{if } V^2\nu/\nu' < c^2 . \qquad (29)$$

$$= C\kappa^{-1/2}(\sigma_g\nu'/2c)^{\kappa-1} \quad \text{if } V^2\nu/\nu' \geq c^2 . \qquad (30)$$

If we adopt the simplifying assumption that $v_g = c$ *always* (the isothermal approximation), then the equations simplify greatly and ν may be put in the following form:

$$\nu(r) = \nu_\odot[\sigma(r)\sigma_g(r)/\sigma_\odot^2]^{\kappa-1} , \qquad (31)$$

where $_\odot$ denotes the values appropriate for the solar neighborhood of our Galaxy. Since $\nu_\odot$ is a constant, it is equal to $\nu(r_\odot, t = 0)$; $\nu(r_\odot, t)$ varies with time t, however. An alternative way to write equation (27) is in terms of the mass fraction in the form of gas $\mathcal{G} = \sigma_g/\sigma$; then

$$\left.\frac{d\mathcal{G}}{dt}\right|_* = -\nu_\odot\left[\frac{\sigma(r)}{\sigma_\odot}\right]^{2(\kappa-1)}\mathcal{G}^{\kappa} . \qquad (32)$$

This form is directly equivalent to the simplified one-zone calculations discussed in TA71, where the rate constant ν is now a function of the surface mass density $\sigma(r)$. Use of equation (31) simply replaces the adjustable parameter C (eq. [26]) by another adjustable parameter $\nu_\odot$.

In the supersonic limit, because $v_g = v_* = c$ always, it might appear that W_g would also be constant. This would be so if star formation occurs in the same proportion to ρ at all z. However, if $\kappa > 1$, then star formation occurs preferentially at the plane $z = 0$ and the gas is preferentially depleted there. Because the gas does not feel the "star pressure," $\rho_* v_*^2$, the gas will redistribute itself as a Gaussian by filling the gas void at $z = 0$. As this process continues, the total mass density at the plane, ρ', builds up and $W_g \propto (\rho')^{-1/2}$ decreases.

If the gas is subsonic, the gas turbulent velocity v_g and equivalent thickness W_g vary with time, and this makes a computation of ν' (eq. [15]) difficult. However, to a first approximation $\nu' \propto \sigma(r)$ because once an appreciable fraction of the mass is locked up in stars, the stars will dominate the sum in equation (15). Consequently,

$$\nu(r) \approx \nu_\odot[\sigma^3(r)\sigma_g^2(r)/\sigma_\odot^5]^{(\kappa-1)/(\kappa+1)} \qquad (33)$$

and

$$\left.\frac{d\mathscr{G}}{dt}\right|_{*} = -\nu_{\odot}[\sigma(r)/\sigma_{\odot}]^{5(\kappa'-1)/2}\mathscr{G}^{\kappa'} \qquad (34)$$

where $\kappa' = (3\kappa - 1)/(\kappa + 1)$. So the subsonic case is almost identical to the sonic case (2.5 in the exponent of $\sigma/\sigma_{\odot}$ instead of 2), subject to a reinterpretation of the meaning of the exponent of $\mathscr{G}$. This is a specific example of the effect discussed by Talbot (1971), to wit, the power κ in the prescription of equation (26) may *not* be directly found by observations without first considering the details of the effects of young stars upon the structure of the gaseous disk.

b) *The MESF Model for the Rate of Star Formation*

By itself the standard power-law prescription for the rate of star formation is not adequate to explain the observed distribution of heavy elements among stars (van den Bergh 1962; Schmidt 1963; TA73*b*). The explanation for this distribution which was discussed by TA73*b* was to assume that stars form more readily in regions of the interstellar gas with higher than average metal abundance (metal-enhanced star formation, or MESF). Talbot (1974) has presented a physical model for the star formation process in which it is argued that the rate of star formation in a unit mass of gas, ν, should be of the form

$$\nu = \nu_0 E\,, \qquad (35)$$

where $\tau_0 = \nu_0^{-1}$ is the characteristic dynamic time scale for the system and E is the "efficiency of star formation," i.e., the fraction of the gas which forms stars during one dynamic time scale. Talbot (1974) discussed a specific formulation for E in terms of the physical properties of the gas (density, pressure, chemical abundances, and heating and ionization mechanisms). The time scale τ_0 is not necessarily defined by local quantities. For the disk models considered in this paper, the appropriate time scale is most probably the mean time between bursts of star formation triggered by the passage of spiral density waves, so we would write

$$\nu_0(r) \approx m[\Omega(r) - \Omega_p]/2\pi \qquad (36)$$

where m is the number of arms, $\Omega(r)$ is the angular velocity of material in circular orbits at r, and Ω_p is the pattern speed (independent of r). If the angular velocities Ω are expressed in units of km s^{-1} kpc^{-1} and ν_0 is expressed in units of aeon^{-1} = (10^9 yr)$^{-1}$, then

$$\nu_0 = 0.163\, m(\Omega - \Omega_p)\,. \qquad (37)$$

For the Galaxy in the neighborhood of the Sun, we adopt $m = 2$, $\Omega(\odot) = 25$ km s^{-1} kpc^{-1}, and $\Omega_p = 13.5$ km s^{-1} kpc^{-1} (Shu 1970) and find $\nu_0(\odot) \approx 3.7$ aeon^{-1}. This agrees well with $\nu_0(\odot) \approx 5$ aeon^{-1} obtained by a similar argument by Talbot (1974).

The factors which determine the pattern speed Ω_p are not clear. It is treated as a parameter in discussions of fitting observations with the density wave theory.

In general $\Omega(r)$ decreases with increasing r; Freeman (1970) gives mathematical expressions and a graph for the exponential disk, and over the range of r which is of interest Ω varies by about a factor of 10. It turns out, however, that in the formulation by Talbot (1974) the expression for E is proportional to an exponential function of ν. The upshot is that when equation (35) is solved for ν, the solution depends upon ν_0 only through a logarithmic term. We will simplify the remaining discussion by leaving ν_0 fixed at 5 aeon^{-1}; this will allow use of models which may be directly compared with the model of Talbot (1974) for the solar neighborhood. Computations with ν_0 factors of 10 larger and smaller alter the results of this paper by less than 30 percent.

Just as with the problem of ascertaining v_g^2, the status of the theory of the heating and ionization of the interstellar gas is uncertain (cf. Dalgarno and McCray 1972; Silk 1973; Gerola, Kafatos, and McCray 1974). This means it is not practical to devise an elaborate model for the MESF process. We adopt the simplified MESF model developed by Talbot (1974) and write

$$E = \exp[(Z_0 - Z_c)/\Delta] \quad \text{if } Z_c \geq Z_0\,, \qquad (38)$$
$$= 1 \quad \text{if } Z_c < Z_0\,,$$

where the parameter Δ is the dispersion in the heavy-element abundance in the interstellar gas, Z_0 is defined by

$$\langle Z_g \rangle = Z_0 + \Delta\,, \qquad (39)$$

and $\langle Z_g \rangle$ is the mass-weighted mean abundance of heavy elements in the gas. The latter comes from the nucleosynthesis computation; it is not free. The quantity Z_c is the "critical" Z for the thermal instability to occur; Z_c is given by

$$Z_c = Z_{\odot}[10^{18}\zeta_{\rm H}/(p_g/k)]\,, \qquad (40)$$

where $\zeta_{\rm H}$ is the primary ionization rate of hydrogen and p_g/k is the gas pressure at the center of the plane in units of cm^{-3} K. The exact details of this model (e.g., the precise figure 10^{18} in eq. [40] and the exact proportionality to $\zeta_{\rm H}$) were based upon a cosmic-ray heating model for the interstellar gas. The qualitative features hold for any steady-state heating model, and a similar behavior may hold on the average for time-dependent models.

We assume that the primary ionization rate of hydrogen is proportional to either the number of massive stars or to their death rate. In either case, we may write $\zeta_{\rm H} = K\nu$, where K is a constant which can be derived from models of the interaction of massive stars with the interstellar gas. We also assume that the gas pressure at the center of the plane is

$$p_g = \rho_g(0)v_g^2 = \tfrac{1}{2}\sigma_g v_g \nu'\,. \qquad (41a)$$

In the supersonic case

$$p_g = \tfrac{1}{2}\pi G\sigma^2(\sigma_g/\sigma) \qquad (41b)$$

since all $v_i = c$ at all times.

The subsonic case is more complex since ν' depends in part upon the stellar velocity dispersion v_* which is frozen at values fixed when the stars form, and in part upon v_g which is changing. In general, for the subsonic case

$$p_g = \tfrac{1}{2}\pi G\sigma^2 \frac{\sigma_g}{\sigma}\left[\frac{v_g}{v_*} + \frac{\sigma_g}{\sigma}\left(1 - \frac{v_g}{v_*}\right)\right]. \qquad (41c)$$

Initially, when $\sigma_g \approx \sigma$ and $v_* \approx v_g$ (because the stars which have just formed from the gas retain the gas dispersion), equations (41b) and (41c) give identical results. Later when $\sigma_g \ll \sigma$, equation (41c) gives p_g lower than the supersonic case by a factor $v_g/v_* = W_g/W_*$.

These considerations allow rewriting equation (40) as

$$Z_c = \frac{2 \times 10^{18}\ \mathrm{K}\ kZ_\odot}{\pi G\sigma\Phi\sigma_g}\,\nu\,, \qquad (42)$$

where $\Phi = 1$ if equation (41b) applies, or Φ equals the square bracket in equation (41c) if that equation applies.

c) *Solar Neighborhood Calibration*

It is natural to employ the solar neighborhood of our Galaxy as a calibration point, for it is the galactic-scale region about which we know the most. For this we need $\sigma_g(\odot)$, $\sigma(\odot)$, $W_g(\odot)$, and the present age of the Galaxy, T.

For the gas parameters we adopt the results of Falgarone and Lequeux (1973). They give numbers which imply $\sigma_{\mathrm{H\,I}}(\odot) = 4.6\ M_\odot\ \mathrm{pc}^{-2}$ and $\sigma_{\mathrm{H\,II}}(\odot) = 0.54\ M_\odot\ \mathrm{pc}^{-2}$; cloud and intercloud column densities each contribute about 50 percent of $\sigma_{\mathrm{H\,I}}(\odot)$. According to Spitzer *et al.* (1973), $f = n(\mathrm{H_2})/n(\mathrm{H})$ varies from less than 10^{-5} along the line of sight for unreddened stars to values ranging from 0.082 to 0.67 for reddened stars. The average of the well-determined f's for reddened stars is 0.375. We adopt $f = 0$ for intercloud material and adopt $f = 0$ and $f = 0.67$ as lower and upper limits for cloud material. Using a "cosmic" abundance of hydrogen of $X_\mathrm{H} = 0.7$, we obtain $7.4 \le \sigma_g(\odot) \le 11.7\ M_\odot\ \mathrm{pc}^{-2}$.

The total surface mass density in the solar neighborhood, $\sigma(\odot)$, is uncertain owing to the uncertainties attendant with the "missing mass" (Oort 1960, 1965). Estimates range from about $80\ M_\odot\ \mathrm{pc}^{-2}$ for analyses based upon the z-distribution of stars (Oort 1965) to values greater than $122\ M_\odot\ \mathrm{pc}^{-2}$ for some dynamic models of the Galaxy (Schmidt 1965; Innanen 1973).

Bearing in mind the 20 percent uncertainties in both $\sigma_g(\odot)$ and $\sigma(\odot)$, we have decided to adopt the following as our standard reference values: $\sigma_g(\odot) = 10\ M_\odot\ \mathrm{pc}^{-2}$, $\sigma(\odot) = 100\ M_\odot\ \mathrm{pc}^{-2}$, and $\sigma_{\mathrm{H\,I}}(\odot) = 0.46\ \sigma_g(\odot) = 4.6\ M_\odot\ \mathrm{pc}^{-2}$. Owing to ignorance of the physics which controls the ratio of neutral atomic hydrogen to total hydrogen, we *assume* $\sigma_{\mathrm{H\,I}} = 0.46\sigma_g$. Without doubt this introduces significant systematic errors in the identification of σ_g from the models and $\sigma_{\mathrm{H\,I}}$ from observations.

The value adopted for $\nu_\odot$ is that value for which the model gives $\sigma_g/\sigma = 0.1$ for the solar neighborhood when the time $t = T$ and where T is defined to be the age of the Galaxy as determined by nucleo-cosmochronology computations (cf. TA73*b* or Schramm 1974).

Radioactive chronologies give approximate limits of $6 \times 10^9 \le T \le 15 \times 10^9$ years (Schramm 1974). Typical models give $13 \pm 3 \times 10^9$ years (e.g., TA73*b* and Talbot 1974). We choose $T = 13 \times 10^9$ years as our canonical age for the Galaxy and, by assumption, other nearby galaxies. The precise value of T is actually unimportant for this paper since the results depend upon T almost solely through the product $\nu_\odot T$. A change in the value for T will cause the required $\nu_\odot$ to be changed in an inverse manner. Whether or not all galaxies are indeed about the same age will not be discussed here.

i) *The Power-Law Birthrate*

In the power-law model for the rate of star formation there are two adjustable parameters, $\nu_\odot$ and κ. The precise value for $\nu_\odot$ depends upon the adopted value of κ as well as upon the details of the initial mass function and the adopted value for T. For the parameters we have adopted, we find

$$\nu_\odot = 0.21\ \mathrm{aeon}^{-1} \text{ if } \kappa = 1$$

$$= 0.43\ \mathrm{aeon}^{-1} \text{ if } \kappa = 1.5$$

$$= 0.92\ \mathrm{aeon}^{-1} \text{ if } \kappa = 2\,.$$

These were obtained with the supersonic model, equation (32). Owing to the approximation leading to equation (34), the subsonic case gives almost identical results provided the exponent κ is reinterpreted as κ'. They were obtained with an IMF with $\zeta = 0.25$ (cf. Appendix).

There are no compelling physical arguments which may be used to derive these numbers from first principles, and we regard them as simply empirical parameters which can be related to C in equation (26) if one has a mind to do so. For example, $C \approx 0.21$ aeon^{-1} if $\kappa = 1$, and $C \approx 2.8\ \mathrm{pc}^3\ M_\odot^{-1}\ \mathrm{aeon}^{-1}$ if $\kappa = 2$.

ii) *The MESF Birthrate*

As presented in the preceding section, the birthrate of stars, ν, has the following parameters: ν_0, Δ, K, and either V or c depending upon which of the two equations (41b, c) is applicable. None of these parameters are actually adjustable parameters at our disposal; in principle they are all determined by the physics of the interstellar gas. This physics is not sufficiently well understood at present to determine these parameters

with precision. For this paper we adopt the following:

1) The rate ν_0 is fixed at the constant value $\nu_0 = 5$ aeon^{-1}. $E(\nu)$ is such a strong function of ν that the results are almost independent of ν_0.

2) The abundance dispersion Δ may be calculated from a theory of how regions enriched by supernova ejecta are mixed with the interstellar gas. TA73*b* and Talbot (1974) discussed this briefly, but at present it is necessary to treat Δ as an adjustable parameter. For the solar neighborhood, the computed distribution of Z over old stars was matched with the observed; and Talbot (1974), using $Z_\odot = 1.7 \times 10^{-2}$, found $\Delta = 2.3 \times 10^{-3}$. It is not clear how Δ should vary with conditions in the gas—increased supernova rates ($\nu > \nu_\odot$) will enhance the composition inhomogeneities through an increase in the source density, but the large supernova rate will enhance the turbulence which will diffusively smooth out composition inhomogeneities. At present we fix Δ at the constant value found for the solar neighborhood.

3) The quantity K is obtained from its definition $\zeta_H = K\nu$ and by equating ionization power per unit volume with the ionizing power available from stars in the unit volume:

$$n_H E_H \zeta_H = \nu \rho_g \frac{\int_0^\infty \psi_m (E_m/m) dm}{\int_0^\infty \psi_m dm}, \quad (43)$$

so that

$$K = (\bar{\mu} m_H / E_H) \int_0^\infty \psi_m (E_m/m) dm, \quad (44)$$

where $\bar{\mu} = \rho_g/(m_H n_H)$ is the mean atomic weight of the gas, E_H is the ionization potential of hydrogen (13.5 eV), and E_m is the net energy which a star of mass m contributes toward ionizing the hydrogen gas. Note that E_m includes all contributions (e.g., cosmic rays, X-rays, etc.) and not just the available ultraviolet photons from, say, OB stars.

There is no simple clear way to compute K owing to uncertainties over what fraction of the total energy output of a star ends up contributing to the ionization of the interstellar hydrogen. This fraction may depend upon the properties of the interstellar gas itself.

As an order-of-magnitude estimate for K (called K_0), we evaluated equation (44) by setting E_m equal to the total energy radiated by a star of mass m while on the main sequence and integrating over the mass interval of 4–60 $M_\odot$. Adopting $\psi_m = 0.25(\mu - 1)m^{-\mu}$ (cf. TA73*a*) and $\bar{\mu} = 1.43$ ($X_H = 0.7$), we find $K_0 = (6.1, 5.7, 4.3) \times 10^3$ for $\mu = (1.3, 1.55, 1.8)$.

In practice we treat K as a free parameter for fitting observations in the solar neighborhood. We rewrite equation (42), expressing σ in units of $M_\odot$ pc^{-2} and ν in units of aeon^{-1}:

$$Z_c = \frac{0.944 Z_\odot K}{\Phi \sigma^2} \frac{\sigma \nu}{\sigma_g}. \quad (45)$$

This expression for Z_c is used with equations (35) and (38) to compute ν; ν is a function of $\langle Z_g \rangle$, the mean heavy-element abundance in the gas. Using this, we find that to fit the distribution of metal abundance in stars in the solar neighborhood we require $K/\Phi \simeq 1.1 \times 10^4$ with an uncertainty of about a factor of 2. Part of the uncertainty is the 20 percent uncertainty in both σ and σ_g, part is the uncertainty in how to treat the variation of Φ with time, and the remainder is the uncertainty in fitting the distribution of Z in stars owing to the uncertainties in the observations. For the present conditions in the solar neighborhood, $W_g \approx 165$ pc (Falgarone and Lequeux 1973), and most of the *visible* mass is contained in dwarf K and M stars with $W_* \approx 420$ pc (assuming a Gaussian distribution and using data from Blaauw 1965). Consequently, the local conditions suggest that at the present time $\Phi \approx v_g/v_* \approx W_g/W_* \approx 0.4$, which means that we require $K \approx 4.4 \times 10^3$, again with an uncertainty of a factor of 2. This is the value of K required by the MESF model. With Weistrop's (1972) M dwarfs, W_* is reduced such that Φ may be about 1.0. In this case, the requirement is $K \approx 1.1 \times 10^4$. The agreement between the required K and the computed K_0 is quite adequate considering the large uncertainties in both.

For the purpose of doing the survey computations in this paper, we adopt $Z_\odot = 1.7 \times 10^{-2}$ and $K/\Phi = 1.1 \times 10^4$; therefore,

$$Z_c(r) = 1.77 \times 10^{-2} \left[\frac{\sigma_\odot}{\sigma(r)}\right]^2 \left[\frac{\sigma(r)}{\sigma_g(r)}\right] \nu; \quad (46)$$

we are assuming K/Φ is rigorously constant. This form is equivalent to the model discussed by Talbot (1974), with the parameters defined in that paper taking the values $n = 1$, $\Delta = 0.2p$, and $\lambda = 7.7$ aeon, where $p = 1.0 \times 10^{-2}$ is the yield of heavy elements.

In order to compare our computed value for K with other estimates of the heating and ionization of the interstellar medium, we note that if the star formation rate ν is expressed in units of aeon^{-1}, then the primary ionization rate of hydrogen ζ_H is $3.17 \times 10^{-17} \nu K$ s^{-1}. Typical values for ν and K for solar neighborhood models are 0.14 aeon^{-1} and 5×10^3; these give $\zeta_H \simeq 2 \times 10^{-14}$ s^{-1}, a value consistent with that required by the observational data and with that obtained by a more careful analysis of the ionizing sources (see Silk 1973). For example, through a detailed consideration of the available ultraviolet photons from observed OB stars outside of H II regions, Torres-Peimbert, Lazcano-Araujo, and Peimbert (1974) obtain $n_H \zeta_H = 1.3 \times 10^{-14}$ s^{-1} cm^{-3} in the plane of the Galaxy. With $n_H \approx 0.5$ cm^{-3}, this means $\zeta_H \approx 2.6 \times 10^{-14}$ s^{-1}.

IV. RESULTS FOR THE FOUR STELLAR BIRTHRATE PRESCRIPTIONS

The preceding section prescribes how variables in the one-zone evolutionary models depend upon the total surface density $\sigma(r)$. We have adopted a constant initial mass function, and we hold constant various uncertain factors such as the parameter Δ which describes the chemical inhomogeneity of the interstellar gas. Consequently, the models presented here

for the evolution of disk galaxies depend only upon $\sigma(r)$ (and upon the time t, of course).

Figure 1 shows some of the results of our computations at the fixed time $t = T = 13$ aeons. The abscissa is logarithmic in the surface density σ. If a galaxy is well represented by an exponential disk (eq. [1]), then the abscissa is linear in the radius $r = R \ln(\sigma_0/\sigma)$; radius increases from left to right. For a given model galaxy the origin of the radial coordinate in figure 1 is determined by the central surface density σ_0. For example, if the central surface density were $\sigma_0 = 403\ M_\odot\ \mathrm{pc}^{-2}$, the origin of the model would be at the point $\ln \sigma = 6$, the point of the abscissa labeled 5 corresponds to $r = R$, etc. Results are shown for four models of the birthrate of stars: two with the power law with $\kappa = 3/2$ and 2, and two with the MESF model using $\Phi = 1$ (the supersonic case where $v_g = c$ always) and $\Phi \propto v_g \propto (vv')^{1/2}$ (the subsonic case). The power-law model can represent the subsonic or supersonic case depending upon how κ is interpreted.

The quantities shown as functions of σ are the surface density of gas σ_g, the combined abundance (by mass) of carbon and oxygen, the ratio of the nitrogen abundance X_N to the carbon-plus-oxygen abundance, the surface density of the rate of formation of stars $\beta = \nu\sigma_g$ (β is the amount of mass converted into stars per square parsec per 10^9 years), and the surface mass-to-light ratio σ/Λ_B (in units of $M_\odot/L_{B\odot}$, where $L_{B\odot}$ denotes the luminosity of the Sun as measured through the B system; we adopt for the sun $M_{\mathrm{bol}} = 4.75$ and $M_B = 5.48$ [Allen 1973]).

The surface luminosity has been computed in each of the *UBV* color bands by using a prescription for the luminosity L_{bol} and effective temperature T_e for individual stars as a function of their age and integrating the luminosities over the initial mass function (IMF) and the history of star formation at each spatial point. The prescription for L_{bol} and T_e and the conversion to *UBV* was essentially identical with that employed by Tinsley (1968, 1973).

The σ/Λ_B curve in figure 1 can be moved up or down at will by changing the lower end of the IMF. The shape, however, is independent of such changes unless one postulates that the IMF varies with σ. The same constant IMF is used for all of these computations (cf. Appendix).

The general features of the variation of quantities with radius r is clear, and these features will reproduce in models with other functions for $\sigma(r)$. Stated in terms of $\sigma(r)$, these results are independent of the radius scale height R and the form of the function $\sigma(r)$. Moving from the low-surface-density exterior of a disk galaxy, σ_g increases to a peak of 10–20 $M_\odot$ pc^{-2}. Based upon conditions in the solar neighborhood, we suggest that the observed H I surface density $\sigma_{\mathrm{H\,I}}$ is of the order of 0.46 σ_g, so the peak in $\sigma_{\mathrm{H\,I}}$ is 4–9 $M_\odot$ pc^{-2}. The predicted peak value depends upon the evolutionary model. The peak occurs where $\sigma(r) \approx$ 30–50 $M_\odot$ pc^{-2}. Interior to the peak, σ_g decreases to a value σ_g (central) $\approx$ 2.4–6 $M_\odot$ pc^{-2}. If the ratio $\sigma_{\mathrm{H\,I}}/\sigma_g$ is a constant, then $\sigma_{\mathrm{H\,I}}$ (central) $\approx$ 1.1–2.8 $M_\odot$ pc^{-2}. The precise central value of $\sigma_{\mathrm{H\,I}}$ depends upon whether this ratio is constant, upon the galactic evolution model, and upon the value of σ in the center. The value of σ_g becomes approximately independent of r for $\sigma \gtrsim 3 \times 10^2\ M_\odot\ \mathrm{pc}^{-2}$.

Note that a peak in β occurs [with β(peak) $\approx$ 1.0–1.5 $M_\odot$ pc^{-2} aeon^{-1}] just inside the peak in σ_g. Near the point at which σ_g becomes flat, β reaches a minimum and then increases with decreasing r. The star formation rate again reaches the value β(peak) if $\sigma \gtrsim 10^3\ M_\odot\ \mathrm{pc}^{-2}$. It is important to note that β varies even though $\sigma_g(r)$ is approximately uniform. The reason is that the volume density of the gas ρ_g increases because the effective thickness W_g decreases for large values of σ (cf. eqs. [15] and [16]). This behavior shows that in general the star formation rate per unit area is not related to the surface density of gas in a simple power-law fashion even if the star formation rate per unit volume is given by a formula like equation (26). This phenomenon will affect the results of analyses undertaken to determine κ, e.g., the work of Sanduleak (1969) and Hartwick (1971) (cf. Talbot 1971). Madore, van den Bergh, and Rogstad (1974) have observational evidence for this effect in M33.

The primary heavy-element abundance X_{CO} rises with decreasing radius until it reaches a peak at a point inside the radius at which β peaks. There is a slight decrease in X_{CO} further in toward higher σ. The absolute level of the abundance of carbon plus oxygen is proportional to the yield p_{CO} which is a weighted integral over stellar mass of the mass fractions ejected as carbon and oxygen (see TA73*a* and TA74 for definitions and a discussion of uncertainty in p_{CO}). The value for the heavy-element yield is uncertain, and this means that the X_{CO} curves perhaps should be translated up or down. The *shape* of the curve is independent of this uncertainty (unless, of course, the IMF varies with σ).

The abundances were computed with yields of $p_{\mathrm{CO}} = 6.7 \times 10^{-3}$ and $q_{\mathrm{N,CO}}/q_{\mathrm{CO,H}} = 7.2$ (see TA73*a*, *b*, TA74, and Appendix).

One might expect to find the greatest surface density of H II regions at the radius where β attains its peak value. At this radius the curves predict abundances of the primary heavy elements which are approximately a factor of 1.5 to 4 less than the highest abundances. Note that the ratio X_N/X_{CO} is closely proportional to X_{CO} over the entire range. This verifies the validity and usefulness of the analytic approximation for secondary species which was discussed in TA73*a*. The models thus predict gradients in the ratio N/O as well as O/H.

In the MESF model the composition gradient in the young stars (labeled y) is not quite as steep as that in the gas as a whole (g). It is not entirely clear, however, which value should be observed in H II regions, since that excited gas initially may have been part of the gas participating in star formation. In that case the hot emission regions would display a composition closer to y than to g.

One of the striking aspects of figure 1 is the qualitative similarity in the solutions for the different models. To distinguish between them by observations

1975ApJ...197..551T

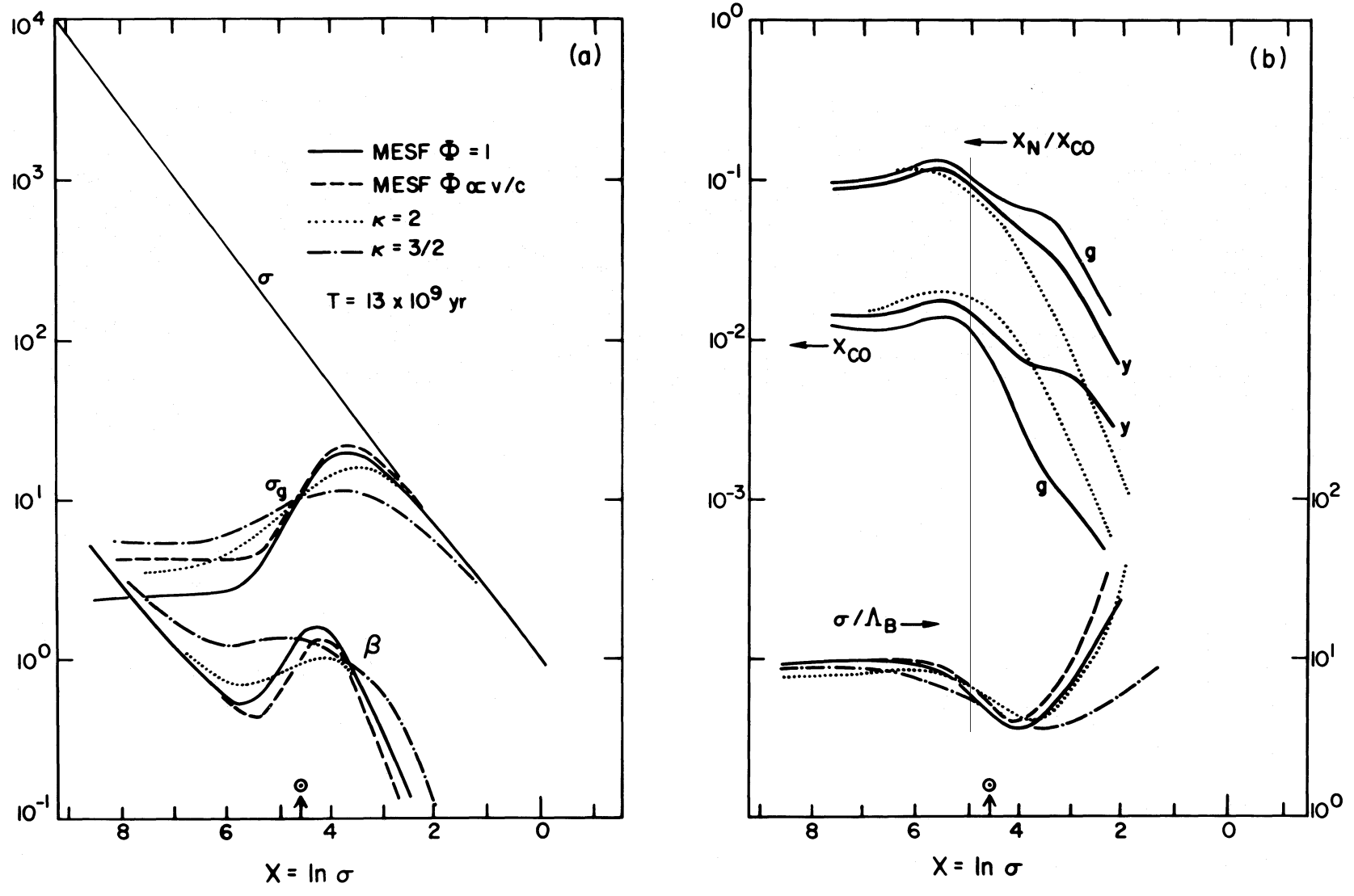

FIG. 1.—Variation of properties of models of disk galaxies is shown with ln σ (surface density of mass) as ordinate. Four models of the rate of star formation are shown: two metal-enhanced star formation (MESF) models, and two power-law models. The surface density of gas (σ_g) is expressed in $M_\odot$ pc^{-2}; the rate of consumption of mass by star formation (β) is expressed in $M_\odot$ pc^{-2} (10^9 yr)$^{-1}$; (σ/Λ_B) is given in units of $M_\odot/L_{B\odot}$. The abundance X_{CO} and the ratio X_N/X_{CO} are shown for the gas (g) and young stars (y) for the MESF $\Phi = 1$ model (the $\Phi \propto v/c$ model falls almost exactly on same curves). Both the $\kappa = 2$ and $\kappa = 3/2$ power-law models fall on the dotted curve (gas and the young stars have the same values).

will require rather detailed information. Considerable care must be taken when making comparisons between these models and observational data which include variations of properties with the azimuthal coordinate. Our models represent approximations to azimuthal averages. Furthermore, our assumptions of no radial flow and negligible spheroidal components are likely to be too restrictive to allow critical comparisons with observational data. For example, gas ejected by dying stars of a spheroidal component may move radially inward.

In view of these considerations, in this paper we will not attempt to use observational data to distinguish between specific models for the stellar birthrate. Instead, we will discuss in some detail the MESF model with $\Phi = 1$, and we will emphasize the qualitative and systematic features of that model. It is evident from figure 1 that the other models will have essentially identical features, with only minor quantitative differences. In table 1 we give numerical values for several quantities of interest so that the reader may compare models quantitatively. In place of β we list a quantity more closely related to observation analysis:

$$\eta(m_L) = 10^3\beta \int_{m_L}^{\infty} \Psi_m m^{-1} dm \,, \qquad (47)$$

which is the number of stars with $m \geq m_L$ formed per kpc^2 in 10^6 years. For the IMF we have adopted (see Appendix)

$$\eta(m_L) = 12.3\beta(m_L/6\ M_\odot)^{-1.35} \,.$$

V. OUR STANDARD FLATTENED EXPONENTIAL GALAXY WITH METAL-ENHANCED STAR FORMATION

a) *Radial Distributions and Integral Properties*

Figure 2 shows the results for the MESF model with $\Phi = 1$. In addition to some of the variables displayed in figure 1, we show the mean heavy-element abundance in all stars, the B surface luminosity, and the colors.

Again we point out that the heavy-element abundance in the gas reaches a maximum just inside the radius at which σ_g attains its peak value. This also is about the place where the colors change sharply and β peaks. The mean heavy-element abundance integrated over all stars of all ages is denoted $\langle Z_s/Z_\odot \rangle$. This is always lower than $Z_y/Z_\odot$ which is the heavy-element abundance in young stars.

Figure 3 shows the differential distribution function $N(Z_s)dZ_s$ which is the fraction of stars with abundance between Z_s and $Z_s + dZ_s$. $N(Z_s)$ is shown for three selected values of σ.

The distribution N for the condition in the solar neighborhood of our Galaxy ($\sigma \approx 100\ M_\odot$ pc^{-2}) agrees well with observations because the Δ parameter in the MSF model has been chosen to do that (Talbot 1974). For low values of σ there is a concentration of stars with Z about equal to the value at 13×10^9 years. On the other hand, for large σ the $N(Z_s)$ distribution is bimodal. There is a concentration at low values of Z_s owing to the very rapid initial star formation, and then a peak at $Z_s \approx 1.4Z_\odot$ which represents the value of Z_s at 13×10^9 years. There is a concentration of stars at this last value because Z_s is held approximately constant by the semiequilibrium process discussed by TA71. These points are made clearer by a study of figure 4 which shows the time development of Z_y, the mean heavy-element abundance of stars formed at time t, and $\mathcal{G} = \sigma_g/\sigma$.

Figure 2 shows the blue photoelectric surface luminosity Λ_B expressed in units of $L_{B\odot}$ pc^{-2} and as μ_B in units of mag arcsec^{-2}. The colors stated are computed from

$$B - V = 2.5 \log \Lambda_V/\Lambda_B + (B - V)_\odot \,,$$

and a similar expression for $U - B$. For reference, in figure 2*b* we indicate the surface brightness of the night sky $\mu_B(S)$ and the surface brightnesses which have been used to define galaxy diameters in various studies: $\mu_B(D) = 24.5$ is the average isophote which defines the diameter of late-type galaxies in the *Reference Catalogue of Bright Galaxies*; $\mu_B(D_m) = 26.6$ is the average isophote at which Holmberg (1958) tabulated D_m, the so-called Holmberg diameter of galaxies; and $\mu_B(D_m) = 27.5$ is the average isophote at the detection threshold on microphotometer tracings of the Mount Stromlo plates and defines D_M, a "maximum" detectable diameter—all of these average isophotes and definitions of diameters were taken from Heidemann, Heidemann, and de Vaucouleurs (1972). In Holmberg's notation $D_m = a$ and the isophote was defined at $\mu \approx 26.5$ mag (pg) arcsec^{-2}.

In order to illustrate the properties of disk galaxies generated by our model, we will discuss a sequence constructed with an exponential distribution of surface mass density σ. The sequence is parametrized by the central surface density σ_0, and the radial variation is displayed in units of R (the e-folding scale height) and $r_{\max}$ which is the position of the maximum of the rotation curve (for a pure exponential disk, $r_{\max} = 2.15R$; a spheroidal component would change this). In the notation of Freeman (1970), $R = \alpha^{-1}$.

For the exponential mass distribution, the velocity at the maximum of the rotation curve is

$$\begin{aligned} V_{\max} &= 0.623\,(G\mathcal{M}/R)^{1/2} \\ &= 3.24\,(\sigma_0 R)^{1/2}\ \mathrm{km\ s^{-1}} \\ &= 2.21\,(\sigma_0 r_{\max})^{1/2}\ \mathrm{km\ s^{-1}} \,, \end{aligned} \qquad (48)$$

where in the latter two expressions σ_0 is given in $M_\odot$ pc^{-2} and R and $r_{\max}$ are in kpc.

The two observational parameters $V_{\max}$ and $r_{\max}$ are sufficient to determine two quantities in a theoretical model. We have chosen a simple, two-parameter mass distribution, $\sigma(r) = \sigma_0 \exp(-r/R)$. A more general class of mass distributions with the same two parameters would be $\sigma(r) = \sigma_0 g(r/R)$, where g is a universal dimensionless function of r/R. Observations of real

Table 1

Properties of One Zone Models with Varying Surface Density

σ	σ Gas	Λ B	U-B	B-V	Bol Corr	η(6)	X CO	X N
MESF Φ = 1								
1.0(1)	9.16	5.81(-1)	-0.220	0.428	1.231	0.87	3.26(-3)	2.72(-5)
2.0(1)	1.53(1)	2.88	-0.199	0.452	1.199	4.16	5.89(-3)	1.29(-4)
3.0(1)	1.86(1)	6.24	-0.176	0.478	1.165	8.57	6.54(-3)	2.25(-4)
4.0(1)	1.96(1)	1.00(1)	-0.152	0.503	1.131	13.05	6.68(-3)	2.68(-4)
5.0(1)	1.89(1)	1.35(1)	-0.124	0.531	1.094	16.68	7.11(-3)	3.16(-4)
7.0(1)	1.53(1)	1.86(1)	-0.053	0.598	1.006	19.65	8.64(-3)	4.66(-4)
1.0(2)	1.00(1)	2.16(1)	0.077	0.704	0.872	16.86	1.16(-2)	8.18(-4)
2.0(2)	3.64	2.61(1)	0.413	0.899	0.657	7.44	1.76(-2)	1.97(-3)
3.0(2)	2.82	3.50(1)	0.518	0.947	0.630	6.54	1.72(-2)	2.05(-3)
4.0(2)	2.67	4.52(1)	0.553	0.962	0.622	7.24	1.61(-2)	1.82(-3)
5.0(2)	2.64	5.41(1)	0.548	0.953	0.606	8.31	1.54(-2)	1.64(-3)
7.0(2)	2.58	7.10(1)	0.527	0.926	0.562	10.60	1.48(-2)	1.46(-3)
1.0(3)	2.51	1.01(2)	0.541	0.929	0.546	14.03	1.45(-2)	1.36(-3)
2.0(3)	2.42	2.09(2)	0.576	0.948	0.548	25.60	1.43(-2)	1.28(-3)
PWR LAW κ = 3/2								
7.0	5.19	1.13	-0.202	0.449	1.202	1.64	2.00(-3)	1.37(-5)
1.0(1)	6.61	2.00	-0.190	0.462	1.185	2.82	2.78(-3)	2.65(-5)
2.0(1)	9.44	5.21	-0.153	0.502	1.132	6.80	5.05(-3)	9.04(-5)
3.0(1)	1.07(1)	8.21	-0.118	0.537	1.085	9.97	6.98(-3)	1.75(-4)
4.0(1)	1.11(1)	1.08(1)	-0.084	0.570	1.044	12.26	8.64(-3)	2.73(-4)
5.0(1)	1.11(1)	1.31(1)	-0.053	0.599	1.007	13.85	1.01(-2)	3.78(-4)
7.0(1)	1.08(1)	1.68(1)	0.005	0.648	0.946	15.68	1.25(-2)	5.96(-4)
1.0(2)	1.00(1)	2.10(1)	0.077	0.703	0.875	16.74	1.51(-2)	9.19(-4)
2.0(2)	7.86	3.22(1)	0.252	0.819	0.751	16.35	1.97(-2)	1.77(-3)
3.0(2)	6.72	4.23(1)	0.349	0.870	0.694	15.81	2.14(-2)	2.28(-3)
4.0(2)	6.08	5.26(1)	0.413	0.901	0.667	15.76	2.17(-2)	2.54(-3)
5.0(2)	5.75	6.26(1)	0.447	0.914	0.647	16.13	2.14(-2)	2.64(-3)
7.0(2)	5.43	8.35(1)	0.492	0.932	0.627	17.58	2.03(-2)	2.59(-3)
1.0(3)	5.35	1.15(2)	0.524	0.943	0.609	20.56	1.86(-2)	2.34(-3)
2.0(3)	5.76	2.23(2)	0.564	0.957	0.590	32.50	1.61(-2)	1.73(-3)

σ	σ Gas	Λ B	U-B	B-V	Bol Corr	η(6)	X CO	X N
MESF Φ = v/c								
1.0(1)	9.59	2.89(-1)	-0.223	0.424	1.236	0.44	1.95(-3)	8.40(-6)
2.0(1)	1.67(1)	2.10	-0.202	0.449	1.203	3.03	5.05(-3)	8.15(-5)
3.0(1)	2.05(1)	5.08	-0.170	0.484	1.156	6.91	6.75(-3)	2.05(-4)
4.0(1)	2.16(1)	8.63	-0.144	0.512	1.121	11.08	6.74(-3)	2.61(-4)
5.0(1)	2.08(1)	1.20(1)	-0.111	0.545	1.077	14.40	7.14(-3)	3.10(-4)
7.0(1)	1.62(1)	1.65(1)	-0.020	0.627	0.969	16.20	8.83(-3)	4.73(-4)
1.0(2)	1.00(1)	1.83(1)	0.155	0.759	0.809	11.88	1.22(-2)	8.78(-4)
2.0(2)	4.72	2.39(1)	0.474	0.927	0.643	5.54	1.73(-2)	1.87(-3)
3.0(2)	4.32	3.41(1)	0.556	0.970	0.643	5.83	1.66(-2)	1.90(-3)
4.0(2)	4.36	4.02(1)	0.500	0.916	0.575	7.04	1.57(-2)	1.72(-3)
5.0(2)	4.33	4.89(1)	0.502	0.909	0.551	8.12	1.53(-2)	1.62(-3)
7.0(2)	4.30	7.20(1)	0.533	0.925	0.547	10.60	1.51(-2)	1.50(-3)
1.0(3)	4.25	1.05(2)	0.558	0.939	0.549	14.15	1.49(-2)	1.42(-3)
2.0(3)	4.22	2.13(2)	0.579	0.950	0.550	26.10	1.46(-2)	1.31(-3)
PWR LAW κ = 2								
7.0	6.67	2.33(-1)	-0.224	0.423	1.237	0.35	3.19(-4)	3.43(-7)
1.0(1)	9.09	6.25(-1)	-0.218	0.430	1.228	0.94	6.36(-4)	1.37(-6)
2.0(1)	1.43(1)	3.30	-0.188	0.465	1.182	4.65	2.25(-3)	1.74(-5)
3.0(1)	1.59(1)	6.69	-0.146	0.510	1.123	8.64	4.29(-3)	6.53(-5)
4.0(1)	1.57(1)	9.50	-0.098	0.558	1.061	11.13	6.39(-3)	1.47(-4)
5.0(1)	1.47(1)	1.16(1)	-0.049	0.603	1.005	12.25	8.37(-3)	2.57(-4)
7.0(1)	1.25(1)	1.43(1)	0.043	0.680	0.911	12.41	1.18(-2)	5.30(-4)
1.0(2)	1.00(1)	1.72(1)	0.162	0.763	0.815	11.35	1.53(-2)	9.63(-4)
2.0(2)	6.34	2.61(1)	0.383	0.884	0.678	9.06	2.00(-2)	1.99(-3)
3.0(2)	5.10	3.63(1)	0.478	0.926	0.635	8.83	2.01(-2)	2.33(-3)
4.0(2)	4.56	4.74(1)	0.529	0.949	0.619	9.35	1.91(-2)	2.30(-3)
5.0(2)	4.23	5.92(1)	0.563	0.967	0.616	10.15	1.81(-2)	2.16(-3)
7.0(2)	3.91	8.40(1)	0.608	0.991	0.619	12.15	1.67(-2)	1.87(-3)
1.0(3)	3.69	1.23(2)	0.648	1.016	0.631	15.39	1.58(-2)	1.61(-3)
2.0(3)	3.46	2.56(2)	0.699	1.048	0.651	27.08	1.50(-2)	1.38(-3)

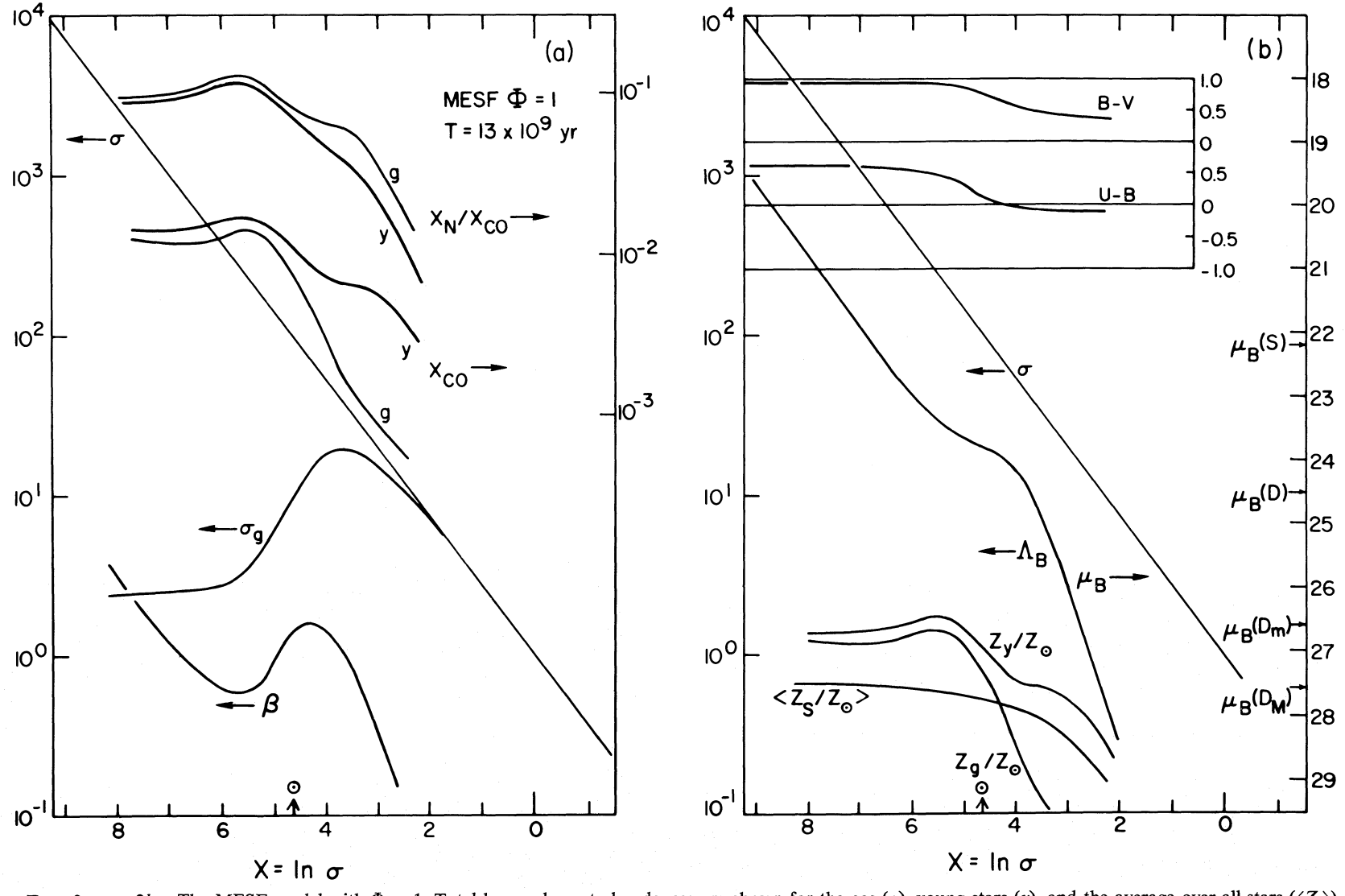

FIGS. 2*a* AND 2*b*.—The MESF model with $\Phi = 1$. Total heavy-element abundances are shown for the gas (g), young stars (y), and the average over all stars ($\langle Z_s \rangle$). The surface density of luminosity is given in units of $L_{B\odot}$ pc^{-2} (Λ_B) and in units of mag arcsec^{-2} (μ_B). Values of μ_B corresponding to the night sky (S), the Reference Catalog diameter (D), the Holmberg diameter (D_m), and the detection threshold (D_M) are shown. The colors given by the ratios of the surface densities of UBV luminosities is illustrated. See fig. 1 for other quantities.

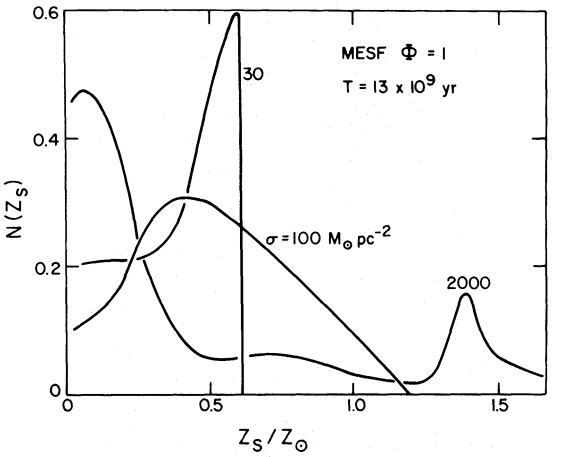

FIG. 3.—Differential distribution of heavy-element abundance over stars at three surface mass densities for the MESF model with $\Phi = 1$.

galaxies suggest that an even more complex function is required which may require more than two parameters. It appears that a general picture for the mass distribution in galaxies involves the superposition of a spheroidal component and a disk component. *Our models refer only to the disk component.* We note that if the strength of the spheroidal component increases with the disk parameter σ_0, a two-parameter family might be preserved.

Tables 2 and 3 and figure 5*a* display the properties of model disk galaxies generated by a sequence in σ_0. All properties are shown in a fashion independent of the radius scale R. In table 2 the rows contain respectively: the ratios of H I mass to total mass, total mass to blue light (solar units), and H I mass to blue light. These are followed by ratios of various radii to R, the radius scale: the radius at which the surface brightness is 26.6 mag arcsec^{-2} (Holmberg radius), $r_h = 0.5D_m$; radial position of the peak of the neutral hydrogen ring r_{ring}; radial position of the peak in the areal density of young stars r_y; and the radius containing one-half the neutral hydrogen H I $\Gamma_{H\,I}$. Also given is a

TABLE 2

PROPERTIES OF EXPONENTIAL DISKS WITH MESF, $\Phi = 1$

σ_0	$M_\odot$ pc^{-2}	50	100	200	700	2000
$\mathcal{M}_{H\,I}/\mathcal{M}$.....		0.40	0.33	0.24	0.11	0.052
$\mathcal{M}/\mathcal{L}_B$.....	$M_\odot/L_{B\odot}$	12.6	7.4	6.1	6.5	7.6
$\mathcal{M}_{H\,I}/\mathcal{L}_B$.....	$M_\odot/L_{B\odot}$	5.1	3.4	1.5	0.72	0.40
r_h/R.....	Holmberg radius	1.3	1.9	2.6	3.8	4.9
r_{ring}/R.....	H I ring	0.24	1.0	1.7	3.0	4.1
r_y/R.....	Young stars	0.0	0.30	0.99	2.2	3.2
$\Gamma_{H\,I}/R$.....	0.5 of H I	1.9	2.2	2.6	3.7	4.5
a.....	r_{ring}/Δ_{ring}	0.10	0.43	0.74	1.3	1.7
$\langle\Lambda_B\rangle$.....	$L_{B\odot}$ pc^{-2}	5.9	7.9	10	15	22
μ_B.....	mag arcmin^{-2}	16.2	15.9	15.6	15.2	14.8
$\langle B-V\rangle$.....		0.47	0.52	0.60	0.73	0.82
$\langle U-B\rangle$.....		−0.18	−0.13	−0.05	0.11	0.27
$\sigma_{H\,I}$(max).....	$M_\odot$ pc^{-2}	9.0	9.0	9.0	9.0	9.0
$\langle\sigma_{H\,I}\rangle_h$.....	$\mathcal{M}_{H\,I}/\pi r_h^2$	24	17	14	10	8.3
$\langle\sigma_{H\,I}\rangle_{0.5}$.....	$0.5\mathcal{M}_{H\,I}/\pi\Gamma_{H\,I}^2$	5.7	7.3	7.4	6.3	5.2
$\mathcal{H}(6)/\mathcal{L}_B$.....	$(10^{10}L_{B\odot})^{-1}(10^2\text{ yr})^{-1}$	1.42	1.30	1.10	0.75	0.52

TABLE 3

RADIAL VARIATION OF INTEGRAL PROPERTIES OF EXPONENTIAL DISKS WITH MESF, $\Phi = 1$

	$M_\odot$ pc^{-2}				
σ_0	50	100	200	700	2000
$\mathcal{M}(r)/\mathcal{L}_B(r)$:					
$r/r_{max} = 0.01$.....	3.7	4.6	7.6	9.9	9.6
$r/r_{max} = 1$.....	8.4	5.0	4.4	7.0	9.3
$r/r_{max} = 2$.....	11.7	6.9	5.6	6.0	7.4
$r/r_{max} = \infty$.....	12.6	7.4	6.1	6.5	7.6
$\mathcal{M}_{H\,I}(r)/\mathcal{M}(r)$:					
$r/r_{max} = 0.01$.....	0.18	0.05	0.01	2(−3)	6(−4)
$r/r_{max} = 1$.....	0.36	0.26	0.14	0.02	2(−3)
$r/r_{max} = 2$.....	0.40	0.32	0.22	0.08	0.02
$r/r_{max} = \infty$.....	0.40	0.33	0.24	0.11	0.05
$(B-V)(r)$:					
$r/r_{max} = 0.01$.....	0.53	0.70	0.90	0.93	0.95
$r/r_{max} = 1$.....	0.46	0.51	0.60	0.85	0.94
$r/r_{max} = 2$.....	0.46	0.51	0.58	0.73	0.84
$r/r_{max} = \infty$.....	0.46	0.51	0.58	0.73	0.82

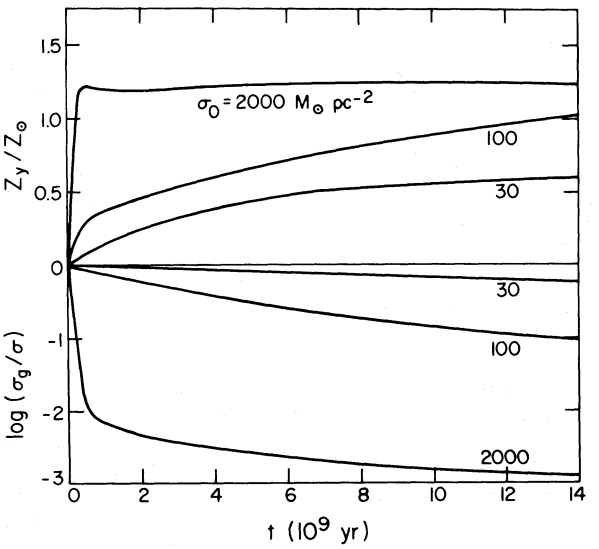

FIG. 4.—Time development of the heavy-element abundance in newly formed young stars (Z_y) and the mass fraction remaining in the form of gas (σ_g/σ); results for three surface mass densities are shown for the MESF model with $\Phi = 1$.

convenient parameter for labeling these models, $a = r_{\rm ring}/\Delta_{\rm ring}$, where $\Delta_{\rm ring}$ is the width of the H I ring (to $\frac{1}{2}$ maximum) which is constant in these models at $\Delta_{\rm ring} = 2.4\ R$. We give the mean surface density of luminosity $\langle \Lambda_B \rangle = \mathscr{L}_B/\pi r_h^2$, the mean surface brightness μ_B in units of mag arcmin^{-2}, and the mean colors for the disks. For the neutral hydrogen surface densities three characteristic quantities are shown: $\sigma_{\rm H\ I}$(max) is the maximum with respect to radius of the H I surface density obtained by an *azimuthal average*, $\langle \sigma_{\rm H\ I} \rangle_h = \mathscr{M}_{\rm H\ I}/\pi r_h^2$, and $\langle \sigma_{\rm H\ I} \rangle_{0.5} = 0.5\mathscr{M}_{\rm H\ I}/\pi \Gamma_{\rm H\ I}^2$. The quantity $\mathscr{H}(6)$ is the integral over the disk of $\eta(6)$ which we discussed in § IV; the ratio $\mathscr{H}(6)/\mathscr{L}_B$ is related to observational data on supernova rates; it is the number of stars born with mass greater than 6 $M_\odot$ per $10^{10}\ L_{B\odot}$ in 10^2 yr.

Table 3 shows the radial variation of three interesting quantities: the integrated-mass to integrated-light ratio $\mathscr{M}(r)/\mathscr{L}_B(r)$, the integrated-hydrogen-mass to integrated-total-mass ratio $\mathscr{M}_{\rm H\ I}(r)/\mathscr{M}(r)$, and the integrated color $(B - V)(r)$. The integrated mass is defined by

$$\mathscr{M}(r) = \int_0^r \sigma(r') 2\pi r' dr'$$

and other quantities analogously. The ratios are shown as a function of $r/r_{\rm max}$ where $r_{\rm max} = 2.15\ R$ is the turnover point in the rotation curve. Very few galaxies have their rotation curves well studied beyond $r/r_{\rm max} \approx 1$; consequently, fair comparisons between observations and models can be made only for carefully defined limits of integration.

The integrated mass-to-light ratios for the models vary only slightly over the interval $B - V \approx 0.46$ to 0.95. The absolute level of these values of $\mathscr{M}/\mathscr{L}$ may be altered by changing the prescription for the lower end of the IMF (cf. Appendix). The displayed variation is due to the effects of a varying extent of depletion of gas into stars and different limits of integration.

This variation in $\mathscr{M}/\mathscr{L}$ occurs with a constant IMF. If close comparisons show discrepancies between observations and these models (with appropriate spherical components added and suitable expressions for $\sigma(r)$ fitted to observed rotation curves), then and only then may one argue for the need to have a variable IMF.

Figure 5*b* shows the surface density distributions of neutral hydrogen observed by 21-cm surveys and numbers of H II regions. The data were derived from the following references: M33: Carranza *et al.* (1968), Huchtmeier (1973), and Rogstad and Shostak (1972). M101: Allen, Goss, and van Woerden (1973), Hodge (1969), and Rogstad and Shostak (1972). M31: Guibert (1974) and Rubin and Ford (1970). M81: Connolly, Mantarakis, and Thompson (1972), and Rots and Shane (1974).

Rogstad and Shostak (1972) give similar curves for three other Scd galaxies which, together with these, display a high degree of homogeneity in their intrinsic properties. Those galaxies all have distributions of H I which are fitted by our exponential model with $a \approx 0.1$ to 0.5. The colors of our models are well within the distribution of colors for Scd galaxies (de Vaucouleurs and de Vaucouleurs 1972).

The observed H I and H II distributions in late type galaxies display qualitative features which agree well with the models. The agreement is remarkably good when one considers that the models are obtained by extrapolating from a solar neighborhood model with no free parameters in the extrapolation except σ_0. The primary discrepancy is that the models have $\sigma_{\rm H\ I}$(max) $\approx 9\ M_\odot\ pc^{-2}$ throughout the sequence whereas there appears to be a trend for $\sigma_{\rm H\ I}$(max) to decrease as a increases. There are several possible causes for this deficiency in the models; at this time we do not know which is the more important, so we just list them. (1) As indicated by the morphological types, the galaxies with more prominent spheroidal components have lower $\sigma_{\rm H\ I}$(max). Since the total mass density is larger than that contained in the disk component alone, the gravitational compression of the disk will be larger than it would be for a pure disk. This will produce a higher rate of star formation which will cause the gas to be consumed more than for a disk alone. (2) On the average, more massive galaxies rotate faster and will have larger values for v_0. If v_0 is larger for earlier types, it might account for the variation; however, as noted before, the models are not strongly sensitive to v_0. (3) The spheroidal component may influence the radial flow of gas; we have assumed no radial flow. Material ejected from stars in the spheroidal component will tend to have low angular momentum about the rotation axis of the galaxy; upon coalescence with the gas in the disk, the angular momentum of the gaseous disk will decrease and hence there will be an inward flow (Biermann 1974). This will cause $\sigma_{\rm H\ I}$(max) to be lower than our current models predict. On the other hand, mass outflow by

1975ApJ...197..551T

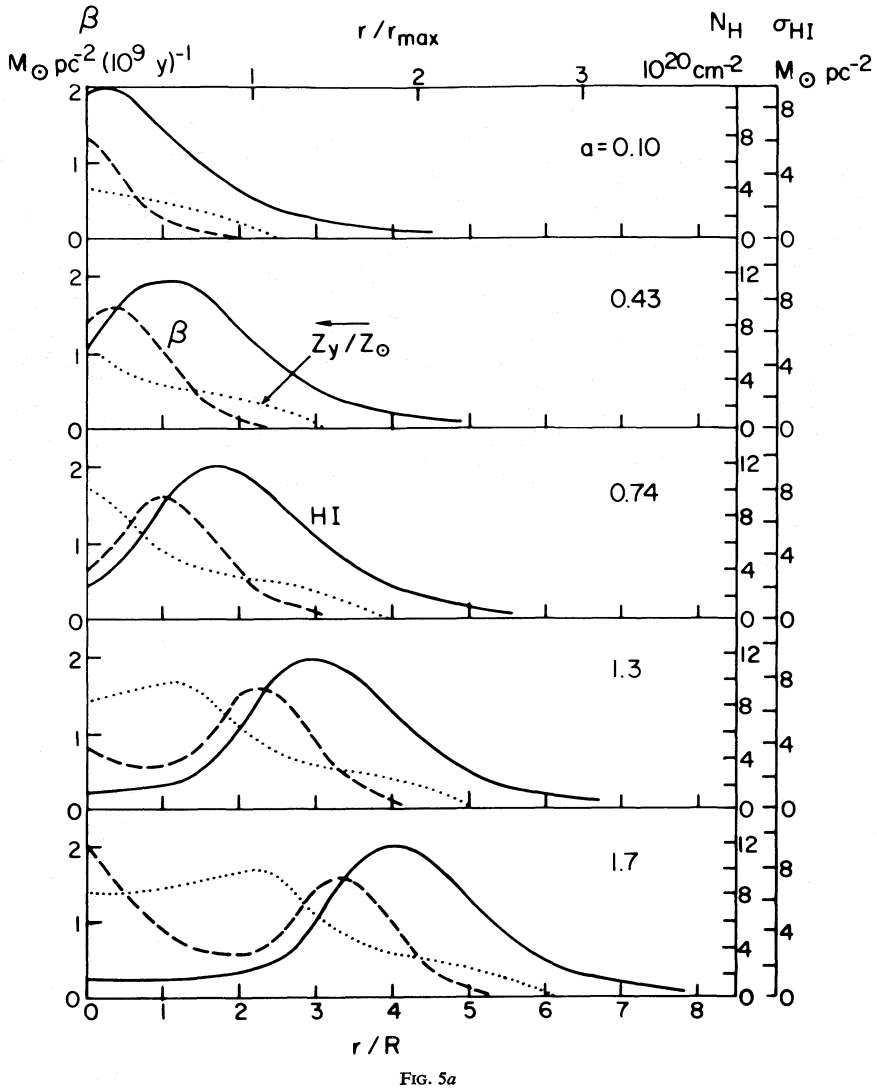

FIG. 5a

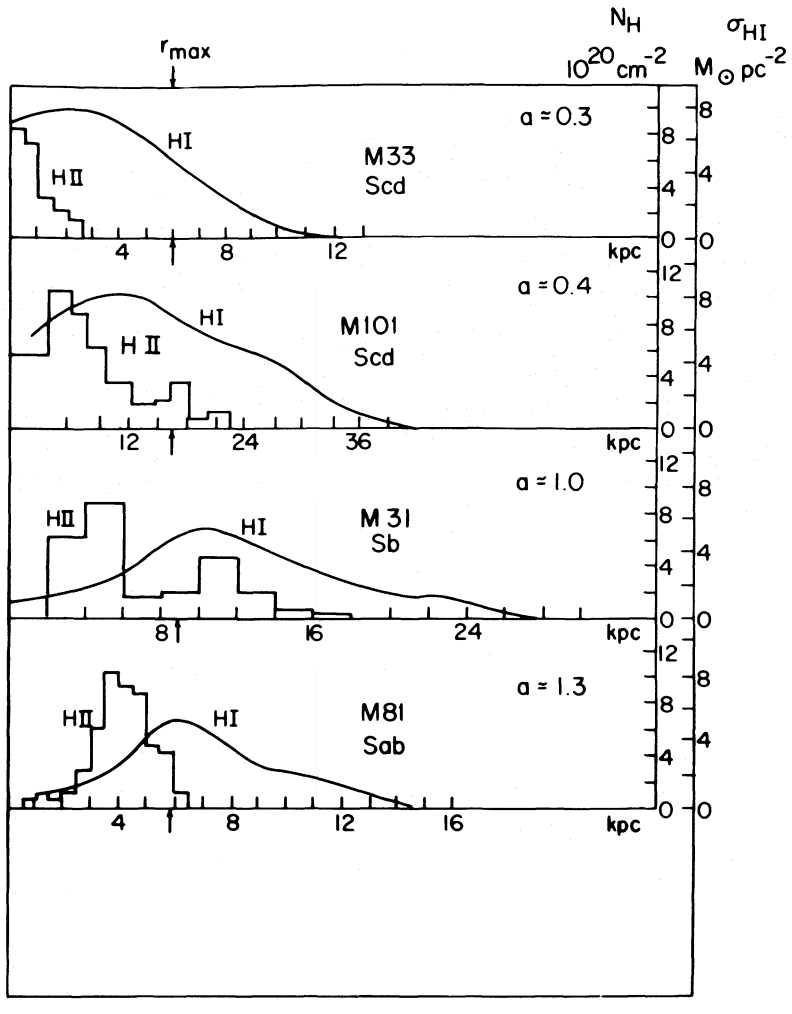

FIG. 5b

FIG. 5a.—A sequence of exponential disk models with increasing σ_0 and increasing $a = r_{ring}/\Delta_{ring}$. The radial distribution is shown for the surface density of H I (under the assumption that $\sigma_{H\,I}/\sigma_g = 0.46$ is constant), the heavy-element abundance in newly formed young stars (Z_y), and the rate of consumption of mass by the formation of stars (β). The latter is expected to be related to (though perhaps not simply proportional to) the surface density of H II regions.

FIG. 5b.—The observed surface densities of H I (21-cm emission) and H II regions (number per unit *area*). For H II regions the units are arbitrary and not necessarily the same for the four galaxies.

explosions in galactic nuclei could have the opposite effect. (4) The fraction of hydrogen which is visible by 21-cm techniques is controlled by uncertain factors. We have assumed a constant value $\sigma_{\text{H I}}/\sigma_g = 0.46$; this is based upon estimates for the solar neighborhood. All 21-cm work (to date at least) has given only lower limits owing to the difficulty in correcting for large optical depths. Furthermore, we have assumed that the relative fractions of the hydrogen in the forms H I, H II, and H_2 are invariant; it is likely that this introduces considerable uncertainty in the ratio $\sigma_{\text{H I}}/\sigma_g$. We regard point (4) as the most significant of those problems.

Figure 6 shows the position of our models (integrals from $\sigma = \sigma_0$ to $\sigma = 0$) in the color-color plane together with mean observed colors from de Vaucouleurs and de Vaucouleurs (1972). The observed colors form a wide band. In addition, for a given Hubble type the colors span a considerable distance along the line representing the means; this is illustrated by the ovals outlining the distribution of points for Sa and Sc galaxies. Since these exploratory calculations use simplified models, our goal is to represent statistically dominant trends. The models easily represent the mean colors by choosing $\mu_2 = 1.35$ in the IMF.

The trends for the variations of color with distance from the center are consistent with those reported by de Vaucouleurs and de Vaucouleurs (1972), and de Vaucouleurs (1961). In the latter reference all galaxies except Sm and Im were found to get bluer as they were integrated outward. In the 1972 reference, types

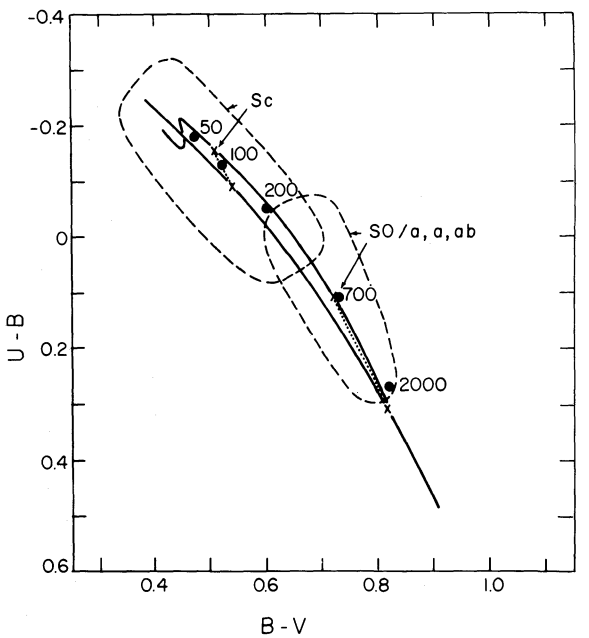

FIG. 6.—The color-color plane distribution of galaxies. The large dots are the integrated colors of disk models developed in this paper; they are labeled with the central surface mass density σ_0 in $M_\odot$ pc^{-2}. The two curves are from de Vaucouleurs and de Vaucouleurs (1972) and illustrate the colors before and after corrections for aperture and ellipticity effects. The two ovals denote the areas occupied by most of the Sc and S0/a,a,ab galaxies.

Sd, Sdm, and Sm were grouped together and stated to be bluer for larger aperture; no statement is made for type Im. Comparisons with the above references suggest that the following rough comparisons may be made: Types Sa/Sb have color aperture relations similar to our $\sigma_0 = 2000\ M_\odot$ pc^{-2} model; Sbc similar to $\sigma_0 \approx 200\ M_\odot$ pc^{-2}, Sc similar to $\sigma_0 \approx 100\ M_\odot$ pc^{-2}. Sd through Im are not clear, but they may correspond to $\sigma_0 \approx 50\ M_\odot$ pc^{-2} where colors are fairly uniform. The problem with attempting these correlations is that individual galaxies may deviate strongly from these relationships. This is partly due to the overall looseness of the correlation between morphological type and color—see § V*c*.

There are only a few available data on the composition gradients in external galaxies, and the interpretations of the data are still somewhat uncertain (Searle 1971; Smith 1973, 1974; Shields 1974). Our models with $\sigma_0 \approx 100$–$200\ M_\odot$ pc^{-2} have abundance gradients which are in the general range estimated for the galaxies M101 and M33—type Scd. The available data do not allow many detailed comparisons, but Smith's (1974) results suggest that some of the N production is primary. He estimates that the oxygen to hydrogen ratio in M101 drops by about a factor of 5 between 10 kpc and 23 kpc. Our model with $\sigma_0 \approx$ 100–200 $M_\odot$ pc^{-2} and $R \approx 8$ kpc gives factors of about 3 to 7. These models give approximately correct distributions of H I and H II (fig. 5) and central colors of $B - V \approx 0.7$–0.9, $U - B \approx 0.15$–0.47. According to de Vaucouleurs (1961), the central colors of M101 are $B - V \approx 0.75$, $U - B \approx 0.21$. This is only an isolated example of the potential of fitting models to specific galaxies. While encouraging, detailed fits will have to wait for more complete models with spherical components and mass distributions based upon individual rotation curves.

Tammann (1974) gives supernova rates per unit luminosity for Sb and Sc galaxies to be 0.69 ± 0.31 and 1.43 ± 0.27; our units here are SN$(10^{10}\ L_\odot)^{-1}$ $(100\ \text{yr})^{-1}$. Taking the mean colors of Sb and Sc galaxies from de Vaucouleurs and de Vaucouleurs (1972) and interpolating in our models, we find rates of 0.87 and 1.34 for Sb and Sc, respectively. This assumes that all stars more massive than 6 $M_\odot$ become supernovae. If we take instead the interval 4–8 $M_\odot$ for supernova progenitors, we find rates which are only 5 percent larger than the stated numbers. Taking the interval 8 $M_\odot$ to infinity, the rates are smaller by 31 percent. Stars above 25 $M_\odot$ contribute less than 10 percent to the rate, although they may contribute half of the nucleosynthesis. These results are similar to those of Arnett and Tinsley (1974), who discuss the supernova progenitor problem in some detail, and Larson and Tinsley (1974).

b) The Manifold of Galaxies

Figure 5*a* and the integral properties given in table 2 show that all intrinsic properties of the models depend upon σ_0 only. By intrinsic properties we mean those independent of the length scale R, e.g., luminosity

per unit area $\langle \Lambda_B \rangle = \mathscr{L}_B/\pi r_h^2$, where $\mathscr{L}_B$ is the total blue luminosity of the model and the r_h is the radius at the isophote employed by Holmberg, $\mu_B \approx 26.6$ mag arcsec^{-2}. Both $\mathscr{L}_B$ and r_h^2 are proportional to R^2, so $\langle \Lambda_B \rangle$ is independent of R.

Quantities which scale with R will be called extrinsic quantities; e.g., $\mathscr{L}_B \propto R^2$, and $r_{max} \propto R$.

Brosche (1973) has argued that the manifold of properties of galaxies can be expressed in terms of two independent parameters, and he found that two appropriate variables appear to be r_{max} and V_{max}. He used this to argue that the manifold of galaxies is produced primarily through the variation in masses $\mathscr{M}$ and total angular momentum $\mathscr{P}$.

Our models show that the primary significant feature is how $\mathscr{M}$ and $\mathscr{P}$ (and any other factors of importance) work together to produce the surface mass distribution $\sigma(r)$. If the distribution is parametrized by two parameters only, then the intrinsic properties will depend primarily upon only the density scale factor σ_0 and the extrinsic properties will scale with R.

For the exponential disks we find the relationships shown in table 4 for the gradients of $\mathscr{L}_B$, color, r_h, and $\mathscr{M}_{H\,I}/\mathscr{M}$. We give the logarithmic gradients with respect to σ_0 and R, and with respect to the two principal axes determined by Brosche, ξ_1 and ξ_2. For this we first transformed our results to the (V_{max}, r_{max})-plane, and then to Brosche's (ξ_1, ξ_2)-plane using his relationship between the latter two coordinate systems. For the gradient in (ξ_1, ξ_2)-space, we give the components of the *unit vector* [denoted by (η_{x1}, η_{x2})] and the magnitude of the gradient vector, N. We list both the gradients given by our model (t) and those determined by Brosche (o). Furthermore, to compare the theoretical with the observed, we give both the ratio of the magnitudes of the gradients, N_t/N_o, and the angle between the two vectors, θ_{ot}. Note that in making our comparisons with Brosche's analysis, the morphological type of a galaxy never enters.

We have not explicitly shown the gradient for $f = \mathscr{M}/\mathscr{L}_B$, but it is easily computed from the gradient for $\log \mathscr{L}_B$ and $\log \mathscr{M} = \log \sigma_0 + 2 \log R +$ constant. The formal result is $\partial(\log f)/\partial(\log \sigma_0) = -0.17$, $\partial(\log f)/\partial(\log R) = 0$. This, however, has little significance in view of the nonmonotonic behavior for $\mathscr{M}/\mathscr{L}_B$ exhibited in table 2. Examination shows that $\mathscr{M}/\mathscr{L}_B$ values are roughly constant while observed values for $\mathscr{M}$ and $\mathscr{L}_B$ each vary by many orders of magnitude. Consequently, the gradient vector for $\mathscr{M}/\mathscr{L}_B$ is the difference between two almost equal vectors. Small errors in either become prominent when the difference is taken. This effect is compounded by the fact that the masses used are generally extrapolations based upon measurements out to only a little beyond r_{max}. The results then vary depending upon the extrapolation procedure used.

The data from which Brosche finds correlations possess large variances, and the level of statistical significance of those correlations is not clear. Consequently, at this time we do not place great weight upon the close agreement between our model and the observations, especially since we know that the models are at best only schematic representations of the mass distribution in actual disk galaxies. Nevertheless, this extremely good fit occurs naturally and with no adjustable parameters, so we feel encouraged to pursue the correlations with more realistic models containing spherical components and σ's derived from rotation curves. More observational studies would be useful also.

c) *The Morphological Type of a Galaxy*

The one very prominent property of flat disk galaxies which we have not discussed in detail is the Hubble type classification or the Yerkes classification system. The Hubble morphological classification depends upon the openness of spiral arms and the strength of the central spheroidal component. To discuss morphological type theoretically requires that spheroidal components and spiral wave theory be incorporated with our disk models. Eventually this will be done.

For the moment we note that although there is a statistically significant correlation between the Hubble type and, e.g., the color of a galaxy, the correlation possesses a large amount of scatter (e.g., fig. 6). Taking the average positions of morphological types in the color-color diagram, it would appear that the Hubble sequence might be explained as a sequence in σ_0. This is attractive until one plots the entire population of individual galaxies of, say, type Sb in this figure—they span the entire locus from $B - V \approx 0.45$ to 0.8, or $\sigma_0 \approx 50$ to 2000 $M_\odot$ pc^{-2} (see figs. 1 and 2 of de Vaucouleurs and de Vaucouleurs 1972).

This lack of a unique correlation between *individual* types and the parameter σ_0 which controls intrinsic

TABLE 4

GRADIENTS IN THE MANIFOLD OF GALAXIES

	MESF Exponential Disk					Brosche (1973)				
x	$\partial x/\partial \log \sigma_0$	$\partial x/\partial \log R$	η_{x1}	η_{x2}	N_t	η_{x1}	η_{x2}	N_o	N_t/N_o	θ_{ot}
$\log \mathscr{L}$.....	1.17	2.0	−0.89	0.46	0.55	−0.98	0.19	0.45	1.2	16°
C.....	...	...	...	...	...	−0.89	−0.46	0.13	0.8	−21
$\langle B - V \rangle$.....	0.218	0	−0.66	−0.75	0.10	...	...	...		
$\log r_h$.....	0.36	1	−0.66	0.75	0.27	−0.74	0.70	0.22	1.2	5
$\log \mathscr{M}_{H\,I}/\mathscr{M}$...	−0.62	0	0.66	0.75	0.29	0.67	0.74	0.43	0.67	−1
									1.0 ± 0.3	0° ± 16°

properties suggests that the type may be governed in part by the parameter R or it may be affected by factors external to our disk model. Clearly the spheroidal component is significant insofar as it is one criterion in the classification scheme. The openness of the spiral arms may be governed by the relative sizes of the spherical and disk components. There may also be significant factors external to the whole galaxy, e.g., the tidal effects of passing companion galaxies.

In summary, we believe that morphological type is not governed solely by the properties of the disk, in spite of the fact that it is about the most outstanding feature of the disk when viewed photographically or by maps of 21-cm radiation.

VI. DISCUSSION

Close comparison between observations of individual galaxies and the predictions of the models presented in this paper are confused by several simplifications in the theoretical models and several inadequacies in the available observational data:

1. Our models do not include a spherical component.
2. The assumed exponential probably does not adequately represent the distribution of mass in the disk component.
3. All short time-scale phenomena affecting the star formation rate (such as spiral density waves and tidal interactions with companions) have been incorporated only in an approximate and average sense.
4. Because of an inadequate knowledge of the physics of the interstellar medium (especially the physics of star formation) we have been forced to extrapolate solar neighborhood conditions.
5. The emphasis of current 21-cm observational efforts has been toward understanding spiral wave structure, i.e., the short time-scale aspects of galactic evolution. The long-time evolution of a galaxy represents a time average of such phenomena. For reasonably regular galaxies one would expect an azimuthal average to approximate a time average. We have found suitable azimuthal averages to be difficult to extract from most of the published observational data.
6. There is only a handful of galaxies for which all of the required data from diverse optical and radio techniques are available.

Although these preliminary calculations involve simplified models, they are successful at describing the qualitative features and statistically dominant trends observed in spiral galaxies. A significant result is that feedback mechanisms in disk models cause the models to be relatively insensitive to the uncertainties in the physics which governs the rate of star formation. Despite their incompleteness, these models may provide a component of a richer, more detailed set of models for the structure and evolution of galaxies.

Special thanks are due Beatrice Tinsley and A. and G. de Vaucouleurs for several valuable conversations. This work was supported in part by NSF grants GP-18335 and GP-32051, and the Research Corporation. The assistance of Professor Harlan Smith and the Department of Astronomy at the University of Texas at Austin is gratefully acknowledged.

APPENDIX

THE INITIAL MASS FUNCTION AND ANALYTIC EXPRESSIONS

In numerical models a unit mass of material forming a generation of stars is distributed among stars of mass m (solar units) by an initial mass function (IMF). We employ an IMF parametrized as

$$\psi_m = \frac{(\mu_2 - 1)(1 - \mu_1)}{\mu_2 - \mu_1} m^{-\mu}, \qquad \text{(A1)}$$

where

$$\mu = \mu_1 < 1 \quad \text{for} \quad m \leq 1$$
$$= \mu_2 > 1 \quad \text{for} \quad m > 1. \qquad \text{(A2)}$$

For certain purposes it is sufficient to specify only the upper portion of the IMF, in which case we may use the form adopted in TA73*a*:

$$\psi_m = \zeta(\mu - 1)m^{-\mu}, \qquad \text{(A3)}$$

where it is to be understood that $\mu = \mu_2 > 1$; ζ is the fraction of the mass contained in stars of $m > 1$.

We have employed a prescription for the luminosity and colors of stars of mass m and age t which is based upon the stellar evolution models of Iben and Stothers —our prescription is essentially identical with that of Tinsley (1968, 1972) and hence is not described in detail. With these models and the observed luminosity function given by Torres-Peimbert *et al.* (1974) we find $\mu_2 = 1.55 \pm 0.46$. This stated uncertainty is the statistical error (95% confidence); there is an unclear error owing to systematic errors in interpretations of observations and the stellar models. To fit the observed *UBV* colors of late-type galaxies requires $\mu_2 \approx 1.35$ (uncertainty is about 0.05). This value is similar to what other investigators have found, e.g. Searle, Sargent, and Bagnuolo (1973). Note that $\mu = 1.35$ is the Salpeter IMF.

The form of the IMF below about 1 $M_\odot$ is uncertain. The luminosity function of van Rhijn gives a mass function with a slope μ_1 around 0.6–0.8; however, in recent years the work of Weistrop (1972, 1974) and others suggests a much steeper slope, at least down to about 0.1 $M_\odot$. For our purposes the *form* of the IMF below 1 $M_\odot$ is not important; we only require that an IMF give appropriate mass-to-light ratios.

In much of her work Tinsley (1968, 1972, 1973) has used a power-law form for the IMF which has a single

power $x = \mu$ and the low end of the IMF is truncated at a lower mass limit m_L. The correspondence between our IMF and her IMF is

$$\zeta = (1 - \mu_1)/(\mu_2 - \mu_1) = (x - 1)m_L{}^{x-1}/x . \quad \text{(A4)}$$

In terms of observational quantities, the primary influences of the IMF are as follows: the shape of the upper portion of the IMF(μ_2) strongly influences the mass-to-light ratio and the yield of the heavy elements. This is easily expressed by use of analytic approximations analogous to those of Tinsley (1973). We find that the stellar mass to light ratio is

$$\frac{\mathcal{M}^*}{\mathcal{L}} \approx \frac{\alpha - \mu_1}{1 - \mu_1} m_0{}^{1-\alpha} \frac{1}{1 + G} , \quad \text{(A5)}$$

where the luminosity of a dwarf star is approximated by $l = m^\alpha$ ($\alpha \approx 4$), m_0 is the mass at turnoff from the main sequence, and G is the ratio of the light from giant stars to that from dwarfs. An expression for the total mass-to-light ratio is also easily obtained, but for most purposes $\mathcal{M}^*/\mathcal{L}$ suffices since usually $\mathcal{M} - \mathcal{M}^* \ll \mathcal{M}$.

The yield of heavy elements is defined in TA73*a* in terms of an integral over m of a production matrix Q_{mij} weighted by ψ_m. The quantity Q_{mij} is the fraction (by mass) of element j which is ejected by a star of mass m in the form of element i. The form of Q_{mij} which we employ was discussed in TA74, and it was shown to give a very satisfactory explanation for the *relative* abundances of most abundant primary heavy elements. For that prescription, the yield of all heavy elements is found to be well approximated by

$$p_z \simeq 0.98[(1 - \mu_1)/(\mu_2 - \mu_1)] \exp(-2.07\mu_2) . \quad \text{(A6)}$$

We caution, however, that this yield is obtained by assuming (1) that all stars undergo the nucleosynthesis production described by TA74 and (2) that the IMF extends with slope μ_2 out to 60 $M_\odot$. Concerning (1), upwards of 50 percent (Paczynski 1971) of massive stars are in binary systems, at least half of which are close binaries where stellar evolution may occur quite differently from single massive stars. Concerning (2), the mass function beyond about 20 $M_\odot$ is uncertain since there are very few such stars and the calibrations of mass are not well determined. For $\mu_2 = 1.55$, 50 percent of the contribution to p_z comes from $m > 35\ M_\odot$. For $\mu_2 = 1.30$, it is about 60 percent! The upshot is that the combined uncertainties in the IMF and the nucleosynthesis products of close binaries mean that the numerical coefficient in equation (A6) may be reduced by a factor of order 2 to 4.

We have chosen the following prescriptions for this paper, and they are kept fixed throughout:

$$\mu_1 = 0.6,\ \mu_2 = 1.35, \quad \text{and} \quad p_z = 1.0 \times 10^{-2} . \quad \text{(A7)}$$

These values were chosen by the following criteria:

a) $\mu_2 = 1.35$ gives *UBV* colors which match observed colors of galaxies.

b) $\mu_1 = 0.6$ together with $\mu_2 = 1.35$ gives $\mathcal{M}/\mathcal{L}_B$ ratios in the range 5–10 $M_\odot$ and specifically $\mathcal{M}/\mathcal{L}_B = 4.63\ M_\odot/L_{B\odot}$ for the MESF $\Phi = 1$ model for the solar neighborhood.

c) $p_z \approx 10^{-2}$ is about that required for a wide range of models to give an appropriate level of Z for the solar neighborhood. The value of p_z obtained with $\mu_1 = 0.6$, $\mu_2 = 1.35$, and our conventional integration over all masses is about 2.7×10^{-2}. Hence, it is possible to reconcile this IMF with heavy-element abundances only if one or both of the assumptions in the previous paragraph fail.

The reader may scale the values for $\mathcal{M}/\mathcal{L}_B$ and abundances for different IMFs by the use of equations (A5) and (A6) to obtain the dependence upon μ_1 and μ_2.

REFERENCES

Allen, C. W. 1973, *Astrophysical Quantities* (3d ed., London: Athlone Press).
Allen, R. J., Goss, W. M., and van Woerden, H. 1973, *Astr. and Ap.*, **29**, 447.
Arnett, W. D., and Tinsley, B. M. 1974, preprint.
Biermann, P. 1974, private communication.
Blaauw, A. 1965, in *Galactic Structure*, ed. A. Blaauw and M. Schmidt (Chicago: University of Chicago Press), p. 435.
Brosche, P. 1973, *Astr. and Ap.*, **23**, 259.
Carranza, G., Courtès, G., Georgelin, Y., Monnet, G., and Pourcelot, A. 1968, *Ann. d'Ap.*, **31**, 63.
Connolly, L. P., Mantarakis, P. Z., and Thompson, L. A. 1972, *Pub. A.S.P.*, **84**, 61.
Dalgarno, A., and McCray, R. A. 1972, *Ann. Rev. Astr. and Ap.*, **10**, 375.
de Vaucouleurs, G. 1959, in *Handbuch der Physik*, ed. S. Flügge (Berlin: Springer), **53**, 311.
———. 1961, *Ap. J. Suppl.*, **5**, 233.
de Vaucouleurs, G., and de Vaucouleurs, A. 1972, *Mem. R.A.S.*, **77**, 1.
Eggen, O. J., Lynden-Bell, D., and Sandage, A. R. 1962, *Ap. J.*, **136**, 748.
Falgarone, E., and Lequeux, J. 1973, *Astr. and Ap.*, **25**, 253.
Freeman, K. C. 1970, *Ap. J.*, **160**, 811.
Gerola, H., Kafatos, M., and McCray, R. 1974, *Ap. J.*, **189**, 55.
Guibert, J. 1974, *Astr. and Ap.*, **30**, 353.
Hartwick, F. D. A. 1971, *Ap. J.*, **163**, 431.
Heidmann, J., Heidmann, N., and de Vaucouleurs, G. 1972, *Mem. R.A.S.*, **75**, 85.
Hodge, P. 1969, *Ap. J.*, **155**, 417.
Holmberg, E. 1958, *Medd. Lunds Obs.*, II, No. 136.
Huchtmeier, W. 1973, *Astr. and Ap.*, **22**, 91.
Innanen, K. A. 1966, *Ap. J.*, **143**, 153.
———. 1973, *Ap. and Space Sci.*, **22**, 393.
Kellman, S. A. 1972, *Ap. J.*, **175**, 353.
Larson, R. B. 1974, *M.N.R.A.S.*, **166**, 585.
Larson, R. B., and Tinsley, B. M. 1974, *Ap. J.*, **192**, 293.
Ledoux, P. 1951, *Ann. d'Ap.*, **14**, 438.
Limber, D. N. 1960, *Ap. J.*, **131**, 168.
Madore, B. F., van den Bergh, S., and Rogstad, D. H. 1974, *Ap. J.*, **191**, 317.
Nordsieck, K. H. 1973*a*, *Ap. J.*, **184**, 719.
———. 1973*b*, *ibid.*, p. 735.
Oort, J. H. 1960, *B.A.N.*, **15**, 45.
———. 1965, in *Galactic Structure*, ed. A. Blaauw and M. Schmidt (Chicago: University of Chicago Press), p. 467.
Paczynski, B. 1971, *Ann. Rev. Astr. and Ap.*, **9**, 183.
Quirk, W. J., and Tinsley, B. M. 1973, *Ap. J.*, **179**, 69.
Rogstad, D. H., and Shostak, G. S. 1972, *Ap. J.*, **176**, 315.
Rots, A. H., and Shane, W. W. 1974, *Astr. and Ap.*, **31**, 245.
Rubin, V. C., and Ford, W. K., Jr. 1970, *Ap. J.*, **159**, 379.
Salpeter, E. 1955, *Ap. J.*, **121**, 161.
———. 1959, *ibid.*, **129**, 608.
Sanduleak, N. 1969, *A.J.*, **74**, 47.

Schmidt, M. 1959, *Ap. J.*, **129**, 243.
———. 1963, *ibid.*, **137**, 758.
———. 1965, in *Galactic Structure*, ed. A. Blaauw and M. Schmidt (Chicago: University of Chicago Press), p. 513.
Schramm, D. N. 1974, *Ann. Rev. Astr. and Ap.*, **12**, 383.
Searle, L. 1971, *Ap. J.*, **168**, 327.
Searle, L., Sargent, W. L. W., and Bagnuolo, W. G. 1973, *Ap. J.*, **179**, 427.
Shu, F. H. 1970, in *Galactic Astronomy*, ed. H.-Y. Chiu and A. Muriel (New York: Gordon & Breach), p. 80.
Shields, G. A. 1974, *Ap. J.*, **193**, 335.
Silk, J. 1973, *Pub. A.S.P.*, **85**, 704.
Smith, H. E. 1973, *Bull. AAS*, **5**, 448.
———. 1974, preprint.
Spitzer, L. 1942, *Ap. J.*, **95**, 329.
Spitzer, L., Drake, J. F., Jenkins, E. B., Morton, D. C., Rogerson, J. B., and York, D. G. 1973, *Ap. J.* (*Letters*), **181**, L116.
Talbot, R. J., Jr. 1971, *Ap. Letters*, **8**, 111.
Talbot, R. J., Jr. 1974, *Ap. J.*, **189**, 209.
Talbot, R. J., Jr., and Arnett, W. D. 1971, *Ap. J.*, **170**, 409 (TA71).
———. 1973*a*, *ibid.*, **186**, 51 (TA73*a*).
———. 1973*b*, *ibid.*, p. 69 (TA73*b*).
———. 1974, *ibid.*, **190**, 605 (TA74).
Tammann, G. 1974, preprint.
Tinsley, B. M. 1968, *Ap. J.*, **151**, 547.
———. 1972, *Astr. and Ap.*, **20**, 383.
———. 1973, *Ap. J.*, **186**, 35.
Torres-Peimbert, S., Lazcano-Araujo, A., and Peimbert, M. 1974, *Ap. J.*, **191**, 401.
Truran, J. W., and Cameron, A. G. W. 1971, *Ap. and Space Sci.*, **14**, 179.
van den Bergh, S. 1962, *A.J.*, **67**, 486.
Vandervoort, P. O. 1970*a*, *Ap. J.*, **161**, 67.
———. 1970*b*, *ibid.*, **162**, 453.
Weistrop, D. 1972, *A.J.*, **77**, 849.
———. 1974, *ibid.*, **79**, 954.

RAYMOND J. TALBOT, JR.: Dept. of Space Physics and Astronomy, Rice University, Houston, TX 77001

W. DAVID ARNETT: Dept. of Astronomy, University of Illinois, Urbana, IL 61801